UCLA/92/TEP/5

High Energy Lepton Hadron Scattering as a Probe of QCD*

R .D. Peccei
Department of Physics, University of California, Los Angeles, CA 90024

Abstract

Tests of QCD in deep inelastic scattering of leptons on hadrons are reviewed and the potential of HERA for exploring particularly the small x region is stressed. Ways to measure the gluon distribution at small x are described and the importance of these measurements is emphasized. The reason for the failure of the Altarelli Parisi and Lipatov equations for very small x phenomena is explained and the physical input underlying the Gribov Levin Ryskin equations, which more correctly account for the low x parton interactions, is discussed. What relevance shadowing and saturation might have for HERA is also briefly touched upon.

*Lectures given at the 1991 SLAC Summer Institute, Stanford, Calif. Aug. 1991. To appear in the Proceedings of the Summer Institute.

These lectures are centered around some of the physics issues that can be explored in high energy lepton hadron scattering. With the commissioning of HERA at DESY in the proximate future, these interactions will be probed to hereto unexplored regions of momentum transfer and Bjorken x. Thus it seems particularly fruitful to discuss here some of the theoretical ideas that have been put forth for this new regime. A useful staring point for my lectures is provided by a review of QCD scaling violations in deep inelastic scattering, using the Altarelli Parisi equations. This not only ties in nicely with the introductory lectures of S. Drell at this school,[1] but it also provides a very natural springboard from which to discuss low x phenomena.

1. Testing QCD Scaling Violations in Deep Inelastic Scattering of Leptons on Hadrons

As is well known[1],[2] quantum chromodynamics (QCD) provides a theoretical justification for the parton model calculations in deep inelastic scattering[3] and predicts logarithmic modifications for the scaling behaviour suggested by Bjorken long ago.[4] In the parton model the deep inelastic scattering cross section for leptons on hadrons can be written as a convolution of the lepton-parton cross section, times the distribution function $f_i(\xi)$ of partons within the hadron.

$$\frac{d\sigma}{dxdy} = \sum_i \int_x^1 \frac{d\xi}{\xi} f_i(\xi) \frac{d\sigma_i}{dx_p dy_p} \quad . \tag{1}$$

Here x and y are the usual (hadronic) variables*

$$x = -\frac{q^2}{2P\cdot q} \quad ; \quad y = \frac{P\cdot q}{P\cdot \ell} \quad , \tag{2}$$

while x_p and y_p are their partonic counterparts,

$$x_p = -\frac{q^2}{2p\cdot q} = \frac{x}{\xi} \quad ; \quad y_p = \frac{p\cdot q}{p\cdot \ell} = y \quad . \tag{3}$$

The kinematics for the process is exemplified in Fig. 1

The lowest order process in QCD is two-body scattering of leptons on quarks and antiquarks. Because the scattering is two-body, the partonic differential cross section is proportional to a δ-function:

$$\frac{d\sigma_i}{dx_p dy_p} \sim \delta(1-x_p) \quad . \tag{4}$$

In turn this implies that, apart from trivial kinematical dependences on q^2, the deep inelastic cross section has no q^2 dependence in this approximation. Thus the

*My metric is $(-1,1,1,1)$, so that for q^2 space-like, as is the case in deep inelastic scattering, then $q^2 > 0$.

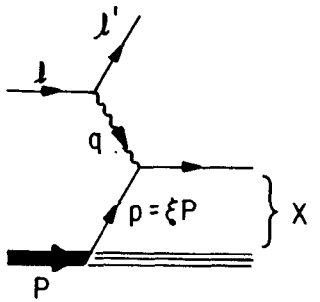

Figure 1: Parton model kinematics for deep inelastic scattering.

lowest order processes in QCD give precisely Bjorken scaling[4] for the hadronic structure functions. For instance, in this approximation, the structure function F_2^{em} for the deep inelastic (electromagnetic) process $ep \to eX$ is just

$$\begin{aligned} F_2^{em}(x;q^2) &= x\sum_i \int_x^1 \frac{d\xi}{\xi}[q_i(\xi)+\bar{q}_i(\xi)]\cdot\left\{e_i^2\delta(1-\frac{x}{\xi})\right\} \\ &= \sum_i e_i^2\,[xq_i(x)+x\bar{q}_i(x)] \quad . \end{aligned} \tag{5}$$

Here $q_i(\xi)$ and $\bar{q}_i(\xi)$ are, respectively, the distribution functions of quarks and antiquarks in a proton, while the term in curly brackets above, containing the characteristic δ-function, is the partonic contribution to the F_2 structure function coming from electron-quark and electron-antiquark scattering.

The lowest order QCD process underlying lepton scattering involves $q + V^* \to q$ and $\bar{q} + V^* \to \bar{q}$ subprocesses, where V^* is a virtual vector boson ($V^* = \{\gamma, W, Z\}$). These subprocesses get modified in higher order QCD, involving the emission of gluons and virtual self energy and vertex gluonic corrections. Both the real and virtual modifications to $0(\alpha_s)$ to V^*-quark scattering are shown in Fig. 2. In addition to these corrections, to $0(\alpha_s)$ the virtual vector boson in deep inelastic scattering can interact directly with a gluon in the hadron producing a quark-antiquark pair, $V^* + g \to q + \bar{q}$. The corresponding graphs for this subprocess are shown in Fig. 3.

The QCD corrections to $0(\alpha_s)$ to the subprocess $V^* + q \to q$ modify the 0^{th} order δ function contribution to the partonic cross section. Schematically, one can write instead of Eq. (4) the expression

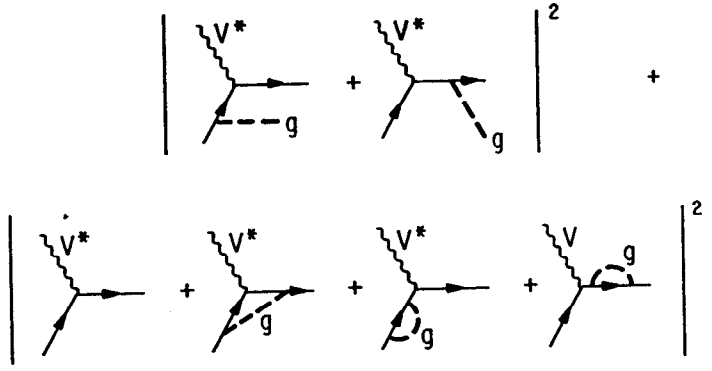

Figure 2: $0(\alpha_s)$ corrections to V^* - quark scattering: a) real corrections ($V^* + q \to q + g$); b) virtual corrections.

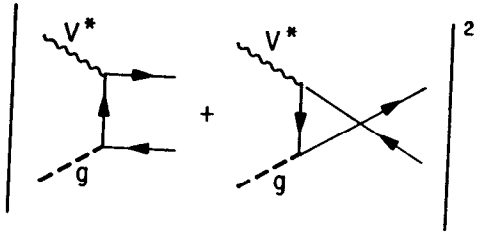

Figure 3: Graphs contributing to the subprocess $V^* + g \to q + \bar{q}$.

$$\frac{d\sigma_i}{dx_p dy_p} \sim [\delta(1-x_p) + \frac{\alpha_s(q^2)}{2\pi}\{P_{qq}(x_p)\ell nq^2 + R(x_p)\}] \quad . \tag{6}$$

These corrections are q^2 - dependent for two reasons:

i) The QCD coupling constant is not a fixed number, but varies depending on which momentum transfer q^2 the partons are being probed with †.

†This "running" of α_s is, actually not seen for the $0(\alpha_s)$ graphs of Fig. 2. It arises from summing up via the renormalization group further corrections to V^* quark scattering like those shown, for example, in Fig. 4.

ii) Gluonic emission has an associated bremsstrahlung spectrum which, upon integration, gives rise to the ℓnq^2 terms in Eq. (6):‡

$$\int^{q^2} \frac{dk_\perp^2}{k_\perp^2} \sim \ell nq^2 \quad . \tag{7}$$

It is clear from Eq. (6) that although the α_s R term is perturbatively small at large momentum transfers, the logarithmic term is **not** small at large q^2 since

$$\alpha_s(q^2)P_{qq}(x_p)\ \ell n\ q^2 \sim P_{qq}(x_p) \quad . \tag{8}$$

So the presence of additional gluon bremsstrahlung appears to vitiate the perturbation expansion! To be able to recover the parton model as the 0^{th} order term in a QCD perturbation series, it is necessary to understand what to do with these terms.

The solution to this conundrum was obtained in the late 1970's when it was understood that these dangerous terms can actually be **factorized** into the parton distribution functions,[5] making these functions also run with q^2. Although I will not enter into the proof of factorization here[6],[5] I will indicate how factorization works in a simple example. For these purposes, let me consider again F_2^{em}. However, now for the parton contribution I will take the $0(\alpha_s)$ expression in Eq. (6), rather than just the δ-function term. Then

$$F_2^{em}(x;q^2) = x\sum_i e_i^2 \int_x^1 \frac{d\xi}{\xi}[q_i(\xi)+\bar{q}_i(\xi)] \cdot [\delta(1-\frac{x}{\xi})+\frac{\alpha_s(q^2)}{2\pi}\{P_{qq}(\frac{x}{\xi})\ell nq^2+R(\frac{x}{\xi})\}] \quad . \tag{9}$$

To the order in α_s that I am working to, Eq. (9) can be rewritten in the following product form

$$\begin{aligned} F_2^{em}(x;q^2) \;=\; & x\sum_i e_i^2 \int_x^1 \frac{d\xi}{\xi}\{[q_i(\xi)+\bar{q}_i(\xi)] + \frac{\alpha_s(q^2)}{2\pi}\int_\xi^1 \frac{d\xi'}{\xi'}P_{qq}(\frac{\xi}{\xi'})[q_i(\xi')+\bar{q}_i(\xi')]\ell nq^2\} \\ & \cdot\{\delta(1-\frac{x}{\xi}) + \frac{\alpha_s(q^2)}{2\pi}R(\frac{x}{\xi})\} \quad . \end{aligned} \tag{10}$$

In this "factorized" form the redefined parton cross section contribution has a well defined perturbation expansion in $\alpha_s(q^2)$. The dangerous term involving ℓnq^2 has been isolated into the parton distribution functions and makes these functions q^2 - dependent:

$$q_i(\xi;q^2) = q_i(\xi) + \frac{\alpha_s(q^2)}{2\pi}\ell nq^2 \int_\xi^1 \frac{d\xi'}{\xi'}P_{qq}(\frac{\xi}{\xi'})q_i(\xi') \quad . \tag{11}$$

‡Some of this dependence also arises from infrared sensitive part of the virtual graphs in Fig. 2.?

In terms of the running parton distribution functions, the hadronic structure functions have a well defined perturbative expansion in $\alpha_s(q^2)$:

$$F_2^{em}(x;q^2) = \sum_i e_i^2 x[q_i(x;q^2) + \bar{q}_i(x;q^2)] + 0(\alpha_s(q^2)) \quad . \tag{12}$$

To the order in α_s we have considered, Eq. (11) is equivalent to the Altarelli - Parisi[7] equation for the quark distribution function

$$\frac{dq_i(\xi;q^2)}{d\ \ell nq^2} = \frac{\alpha_s(q^2)}{2\pi}\int_\xi^1 \frac{d\xi'}{\xi'} P_{qq}(\frac{\xi}{\xi'}) q_i(\xi';q^2) \quad . \tag{13}$$

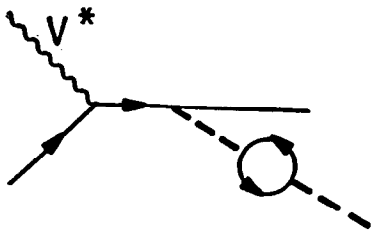

Figure 4: Typical high order graph which contributes to the running of $\alpha_s(q^2)$ in Eq. (6) .

Actually, this equation is not quite complete since to $0(\alpha_s)$ there is an additional contribution to F_2^{em} coming from the subprocesses $g + V^* \rightarrow q + \bar{q}$ depicted in Fig. 3. These contributions provide an additional term for the Altarelli Parisi equation, proportional to the distribution of gluons within a proton. Thus the correct Altarelli Parisi equation for the quark distribution function is not Eq. (13) but

$$\frac{dq_i(\xi;q^2)}{d\ \ell nq^2} = \frac{\alpha_s(q^2)}{2\pi}\int_\xi^1 \frac{d\xi'}{\xi'}[P_{qq}(\frac{\xi}{\xi'}) q_i(\xi';q^2) + P_{qg}(\frac{\xi}{\xi'}) g(\xi';q^2)] \quad . \tag{14}$$

Here the, so called, splitting functions $P_{qq}(\frac{\xi}{\xi'})$ and $P_{qg}(\frac{\xi}{\xi'})$ give the probability, respectively, of finding a quark with momentum fraction ξ inside either a quark or a gluon of momentum fraction ξ'. Corresponding to Eq. (14) there is also an analogous Altarelli Parisi equation describing the q^2 evolution of the gluon distribution function, from branching processes of gluons and quarks. This equation

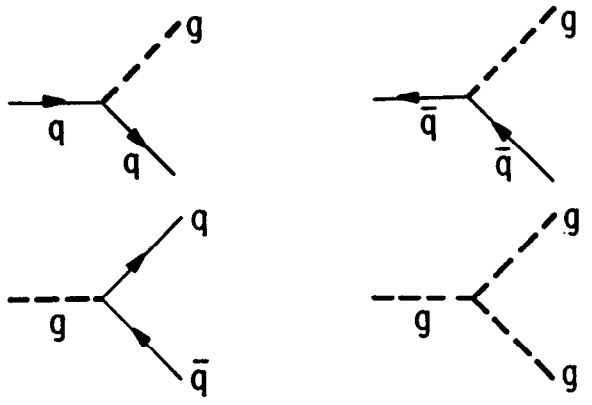

Figure 5: Basic QCD processes giving rise to the splitting functions (16).

reads

$$\frac{dg(\xi;q^2)}{d\ \ell nq^2} = \frac{\alpha_s(q^2)}{2\pi}\int_\xi^1 \frac{d\xi'}{\xi'}\left[P_{gg}(\frac{\xi}{\xi'}) g(\xi';q^2) + \sum_i P_{gq}(\frac{\xi}{\xi'})[q_i(\xi';q^2) + \bar{q}_i(\xi';q^2)]\right] \quad , \tag{15}$$

where $P_{gg}(\frac{\xi}{\xi'})$ and $P_{gq}(\frac{\xi}{\xi'})$ are the corresponding splitting functions for gluons and quarks of momentum fraction ξ' to become a gluon of momentum fraction ξ.

The splitting functions just reflect the basic QCD processes, shown in Fig. 5, by which quarks and gluons of higher momentum becomes quarks and gluons of lower momentum. The splitting functions are independent of quark flavor and they can be determined by computing the coefficients of the ℓnq^2 term in the appropriate parton scattering subprocesses. I record here for later use the expression that one deduces in lowest order for each of the four splitting functions in Eqs. (14) and (15)[7,2]:

$$P_{qq}(z) = c_F\left[\frac{1+z^2}{(1-z)_+} + \frac{3}{2}\delta(1-z)\right] \quad (16a)$$

$$P_{qg}(z) = \frac{1}{2}\left[z^2+(1-z)^2\right] \quad (16b)$$

$$P_{gq}(z) = c_F\left[\frac{1+(1-z)^2}{z}\right] \quad (16c)$$

$$P_{gg}(z) = 2c_A\left[\frac{z}{(1-z)_+} + \frac{1-z}{z} + z(1-z)\right] + \frac{11c_A - 2f}{6}\delta(1-z). \quad (16d)$$

Here f is the number of quark flavors, while c_A and c_F are weight factors associated with the gluons and the quarks [$c_A = 3$ and $c_F = \frac{4}{3}$ for QCD]. The + instruction in the denominators in Eqs. (16) removes the singularity as $z \to 1$ by a principal value prescription[7]:

$$\int_0^1 dz \frac{f(z)}{(1-z)_+} = \int_0^1 dz \frac{f(z)-f(1)}{1-z} \quad . \quad (17)$$

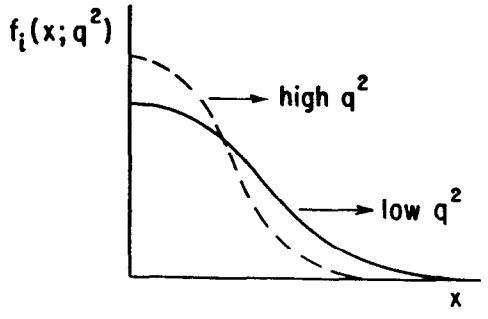

Figure 6: Evolution with q^2 of the parton distribution functions which follows for the Altarelli Parisi equations.

The Altarelli Parisi equations encompass all the information coming from QCD for the deep inelastic region, where $q^2 \to \infty$ and $-q \cdot P \to \infty$, but x is fixed. The predictions one obtains for the hadronic structure functions using these equations, along with the QCD corrected parton cross sections, are entirely equivalent to those obtained using the more formal operator product expansion methods.[8] However, in many ways the physics of what is going on is much clearer in the Altarelli Parisi language. As q^2 increases, when a point-like object probes a hadron it has less and less probability of scattering off a parton at large x, for partons of larger momentum fraction naturally evolve by gluon emission, or quark-antiquark production, into partons of smaller momentum fraction. From the Altarelli Parisi equations one sees that, as q^2 increases, the parton distribution functions at large x are depleted, while there is a concomitant enhancement of small x partons. This behavior is shown schematically in Fig. 6.

The evolution with q^2 of the parton distribution functions produces a logarithmic variation with q^2 of the hadronic structure functions. This variation is a violation of Bjorken scaling. Furthermore, the specific behaviour with q^2 predicted for the structure functions is a direct test of QCD. Because of the presence of the gluon distribution function, there is an important practical difference between, so called, **singlet** and **non singlet** hadronic structure functions. Non singlet structure functions always involve the difference of quark and/or antiquark distributions. Because the splitting functions are independent of the quark flavor, or whether one is dealing with a quark or an antiquark, non singlet structure functions are independent of the gluon distribution function. For example, a structure function like xF_3 for charged current neutrino scattering off isoscalar targets, involves the difference between quark and antiquark distributions for u and d quarks. Thus

$$[xF_3(x;q^2)]^{cc}_{\text{isoscalar}} = x\left[u(x;q^2) + d(x;q^2) - \bar{u}(x;q^2) - \bar{d}(x;q^2)\right] \quad (18)$$

is a non singlet structure function. As a result xF_3, as well as any other non singlet structure functions, $f^{NS}(\xi;q^2)$, obeys the simple Altarelli Parisi equation given in Eq. (13):

$$\frac{df^{NS}(\xi;q^2)}{d\,\ell nq^2} = \frac{\alpha_s(q^2)}{2\pi}\int_\xi^1 \frac{d\xi'}{\xi'} P_{qq}\left(\frac{\xi}{\xi'}\right) f^{NS}(\xi';q^2) \quad . \quad (19)$$

Singlet distribution functions - which we will denote by $f^S(\xi;q^2)$ - on the other hand always obey the coupled Altarelli Parisi equations, Eqs. (14) and (15), which involve the gluon distribution function. Because the evolution of these distributions needs knowledge of the gluon distribution function, QCD tests involving singlet structure functions are more challenging. In general, most hadronic structure functions will involve both singlet and non singlet pieces, so to do appropriate QCD tests one also needs to know something about the gluon distribution function. For example, assuming for simplicity that only the u and d quarks distributions are relevant in the proton, one can write F_2^{em} as the following sum of singlet and non singlet pieces:

$$\begin{aligned} F_2^{em}(x;q^2) &= \sum_i e_i^2 x[q_i(x;q^2) + \bar{q}_i(x;q^2)] \\ &= \frac{5}{18}x[u(x;q^2) + \bar{u}(x;q^2) + d(x;q^2) + \bar{d}(x;q^2)] \\ &+ \frac{1}{6}x[u(x;q^2) + \bar{u}(x;q^2) - d(x;q^2) - \bar{d}(x;q^2)] \quad . \end{aligned} \quad (20)$$

Deep inelastic data shows clearly the qualitative behaviour expected from QCD, in which at low x the structure functions grow with q^2, while they decrease

with q^2 for large x. This can be appreciated from the compilation of data on F_2 obtained in deep inelastic scattering of neutrinos and muons on an isoscalar target[§], shown in Fig. 7. Quantitative tests of QCD, however, are more difficult to perform because:

i) Present data is still taken at rather low values of q^2.

ii) There is some discrepancy between the various experiments, particularly at low values of x.

iii) Structure functions with a singlet component are rather sensitive to the poorly known gluon distribution, particularly at low x.

Nevertheless, particularly when one restricts oneself to data taken by an individual collaboration and does not combine data sets, there appears also to be quantitative agreement with QCD predictions.

I will not delve on how well QCD is being tested with present deep inelastic data, as this has been discussed in much more detail in the lecture of Traudl Hansl Kozanecka[10] in this school, as well as in the seminar by Mishra[11] on the new results from CCFR. Nonetheless, I would like to make a few remarks on these matters to make these lectures somewhat self contained. Present day data encompasses still a rather limited q^2 range ($q^2 \lesssim 100$ GeV^2). Furthermore, it is questionable how far down in q^2 one can push the comparison of data with QCD without the inclusion of non leading $1/q^2$ corrections (the, so called, higher twist terms). Given these facts, it is understandable that the QCD tests so far performed with deep inelastic data essentially reduce to checking that the structure function's q^2 - variation, at different x values, is described by the same **scale parameter** which enters in $\alpha_s(q^2)$.

The running coupling constant $\alpha_s(q^2)$, including terms of order $(\ell n\ q^2)^{-2}$, is given by the expression[2]

$$\alpha_s(q^2) = \frac{1}{b\ell n\ q^2/\Lambda^2}\left\{1 - \frac{b'\ell n\ \ell n\ q^2/\Lambda^2}{b\ell n\ q^2/\Lambda^2} + \cdots\right\} \quad , \tag{21}$$

where the constants b anb b', which depend on the number of flavors f which are active, are

$$b = \frac{1}{4\pi}[11 - \frac{2}{3}f] \quad ; \quad b' = \frac{1}{4\pi}\left[\frac{306 - 38f}{33 - 2f}\right] \quad . \tag{22}$$

The scale parameter Λ in Eq. (21) can be extracted from deep inelastic experiments from the evolution of the structure functions with q^2. The $0\Big((\ell n\ q^2)^{-2}\Big)$ corrections in Eq. (21), as well as the non leading logarithmic's corrections to the evolution

[§]The neutrino and muon data can be plotted together for an isoscalar target after multiplying the muon data by $\frac{18}{5}$, to account for the quark charges [cf Eq. (20)].

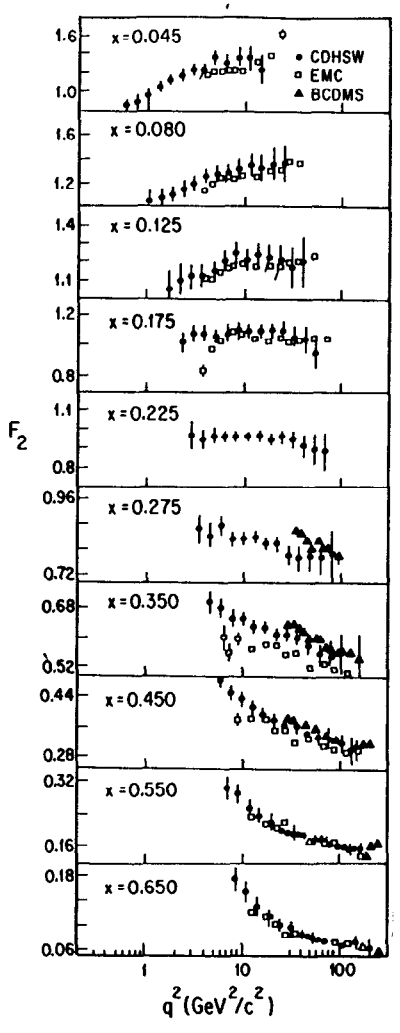

Figure 7: Compilation of data on F_2 for various values of x, as a function of q^2. Adapted from.[9]

equations, are important to specify precisely the Λ parameter one is measuring. The particular parameter one usually quotes from analyses of deep inelastic data is $\Lambda_{\overline{MS}}(f=4)$, where $\overline{MS}$ denotes the renormalization scheme used to compute the nonleading logarithmic corrections[12] and 4 flavors (u, d, s and c) are taken as active. The way this analysis is done by the various experimental collaborations is to evolve the structure functions measured at a given q^2 value ($q^2 = q_0^2$) to a larger q^2 value, keeping Λ as parameter to be determined from the fit. For non singlet structure functions this procedure requires, in principle, no further inputs. However, for the singlet case, in addition, one must input some assumed gluon distribution at q_0^2 and there results - in general - some correlation between the value of Λ extracted and the functional form of $g(x;q_0^2)$ assumed.

Let me expand briefly on each of the points alluded to above. The importance of including corrections beyond the leading order to properly fix Λ can be best appreciated by considering not the structure functions themselves, but their moments.[8] For simplicity, let me just examine the non singlet equation, Eq. (19), and consider the moments of the non singlet distribution $f^{NS}(\xi;q^2)$:

$$M_n(q^2) = \int_0^1 \frac{d\xi}{\xi}\xi^n f^{NS}(\xi;q^2) \quad . \tag{23}$$

Defining the moments of the splitting function $P_{qq}(\xi)$ by

$$A_n = \int_0^1 \frac{d\xi}{\xi}\xi^n P_{qq}(\xi) \quad , \tag{24}$$

it is easy to see that Eq. (19) implies the following simple differential equation for the moments

$$\frac{dM_n(q^2)}{d\ \ell n q^2} = \frac{\alpha_s(q^2)}{2\pi} A_n M_n(q^2) \quad . \tag{25}$$

Using for $\alpha_s(q^2)$ only the lowest order term in $(\ell n\ \ q^2)^{-1}$ in Eq. (21), it follows that the moments depend on q^2 as powers of $\ell n q^2$:

$$M_n(q^2) \ \sim\ [\ell n q^2/\Lambda^2]^{\frac{A_n}{2\pi b}} \quad . \tag{26}$$

However, if one wants a more accurate description it is necessary both to include the higher order terms in Eq. (21), as well as include $0(\alpha_s)$ corrections to the parton model. If one does not drop the $0(\alpha_s)$ terms, then it no longer is true that the hadronic structure functions are the same as the parton distribution functions [cf. Eq. (12)]. If we denote the non singlet hadronic structure function by $F^{NS}(x;q^2)$ and its moments by $\mathcal{M}_n(q^2)$ then, including $0(\alpha_s)$ corrections, one has

$$F^{NS}(x;q^2) = f^{NS}(x;q^2) + \alpha_s(q^2)\tilde{f}(x;q^2) \tag{27}$$

and

$$\mathcal{M}_n(q^2) = M_n(q^2)\left[1 + \alpha_s(q^2)B_n\right] \quad . \tag{28}$$

The function $\tilde{f}(x;q^2)$ and the coefficient B_n are dependent on the scheme one adopts for renormalizing the theory, with a convenient scheme being the minimal subtraction (MS) scheme of 't Hooft,[13] or its modification - the $\overline{MS}$ scheme.[12] Similarly, in the Altarelli Parisi equation Eq. (19) for the non singlet distributions, the splitting functions P_{qq} will have $0(\alpha_s)$ corrections, beyond the leading terms given in Eq. (16a). These need to be calculated in the same scheme in which $\tilde{f}$ was extracted. Thus, including $0(\alpha_s)$ corrections, the parton moments are given by

$$M_n(q^2) = M_n(q_0^2)\left[\frac{\alpha_s(q_0^2)}{\alpha_s(q^2)}\right]^{\frac{A_n}{2\pi b}}\left\{1 + [\alpha_s(q^2) - \alpha_s(q_0^2)]Z_n\right\} \quad . \tag{29}$$

Here the coefficient Z_n - as well as the coefficients B_n above - are calculable, but depend on the renormalization scheme. Finally, using both Eqs. (28) and (29), and including the $0((\ell n q^2)^{-2})$ term in Eq. (21), the moments of the hadronic structure functions are seen to obey the following equation

$$\mathcal{M}_n(q^2) = C_n\left[1 + \frac{R_n(q^2)}{4\pi b \ell n\ q^2/\Lambda^2}\right](\ell n\ q^2/\Lambda^2)^{\frac{A_n}{2\pi b}} \quad , \tag{30}$$

where

$$R_n(q^2) = B_n + Z_n - 2\frac{b'}{b}A_n \ell n\ \ell n\ q^2/\Lambda^2 \quad . \tag{31}$$

The term involving $R_n(q^2)$ in Eq. (30) contains the first non leading corrections to the lowest order QCD expectation for the structure function moments, Eq. (26). Including these corrections, calculated in a particular scheme, one **specifies** which scale parameter one uses. Indeed, it is easy to see that a change in Λ implies a change in $B_n + Z_n$ and vice versa. For if $\Lambda \to e^k\Lambda$, then

$$R_n(q^2) \to \bar{R}_n(q^2) = R_n(q^2) + 4A_n k \quad , \tag{32}$$

so that $B_n + Z_n \to B_n + Z_n + 4A_n k$. I note, parenthetically, that it is possible to invent schemes where to $0(\alpha_s)$ **some** structure function is the same as the corresponding parton distribution function. That is, one can invent a scheme where, for example, $B_n = 0$ so that $\mathcal{M}_n = M_n$ and the non singlet structure function is the same as the non singlet parton distribution: $F^{NS}(x;q^2) = f^{NS}(x;q^2)$. In practice, actually this is done for $F_2^{em}(x;q^2)$, where in the, so called, DIS scheme[14]

$$F_2^{em}(x;q^2) = \sum_i e_i^2 x[q_i(x;q^2) + \bar{q}_i(x;q^2)] + 0(\alpha_s^2) \quad . \tag{33}$$

However, because one can make such an identification for **only** one structure function, for example, in the DIS scheme F_L does indeed contain $0(\alpha_s)$ corrections to the parton model formulas. Because of this, I believe it is preferable to use the $\overline{MS}$ scheme, where the corrections to **all** structure functions and parton distributions are treated in a symmetrical fashion [i.e., one has both B_n and Z_n corrections, in the language of Eq. (31)].

Fits of deep inelastic data for non singlet structure functions can, in principle, provide a better value for $\Lambda_{\overline{MS}}(4)$ than those involving singlet structure functions. Because both the gluon and non valence quark distributions are concentrated at small x, one can, in fact, do a non singlet fit for F_2^{cm} for large x. Such a fit, for the variation of F_2^{cm} with q^2, has been done by the BCDMS collaboration[15] and is displayed in Fig. 8 for both their Carbon and Hydrogen data. From these fits the collaboration deduces a value

$$\Lambda_{\overline{MS}}(4) = (220 \pm 55)\ MeV \quad (BCDMS) \tag{34}$$

for the QCD scale parameter. This value is compatible with the value that the CDHSW collaboration extracts by examining the xF_3 distribution in neutrino deep inelastic scattering. However, the central value obtained by the CDHSW collaboration[9] for $\Lambda_{\overline{MS}}$ is about a factor of two smaller $[\Lambda_{\overline{MS}}(4) = (100 \pm \frac{90}{60})\ MeV]$ and the overall fit - at least to my eyes - looks rather poor. Indeed, it appears to me that probably this value should be disregarded, particularly in the light of the new data of CCFR.[11] Although no official value for $\Lambda_{\overline{MS}}(4)$ has been given yet by the CCFR collaboration, it is clear that their data is much more compatible with the BCDMS value for $\Lambda_{\overline{MS}}(4)$ given in Eq. (34).

Further evidence that $\Lambda_{\overline{MS}}(4)$ is closer to 200 MeV, rather than 100 MeV, comes from the singlet analysis done by BCDMS. Fig. 9 shows the variation of $d\ell nF_2/d\ell nq^2$ with x for the muon deep inelastic scattering data on Hydrogen of BCDMS.[15] As can be seen, the data is well fit by the solid curve which corresponds to $\Lambda_{\overline{MS}}(4) = 220\ MeV$. The slope of the F_2 variation with ℓnq^2 sharpens as $x \to 0$ due to the gluon distribution in the proton and the figure shows the importance of this distribution at small x. The BCDMS fit assumed that at $q_0^2 = 5\ GeV^2$ the gluon distribution could be parameterized by

$$xg(x;q_0^2) = A_g(1-x)^{\eta_g}\ , \tag{35}$$

with $\eta_g = 8$.

Even though a value of $\Lambda_{\overline{MS}}(4)$ around 200 MeV is perfectly compatible with other tests of QCD carried out with other hard scattering data,[16] in deep inelastic scattering the value of $\Lambda_{\overline{MS}}$ extracted appears to be correlated with the softness of the gluon distribution. This is nicely demonstrated by the recent analysis of Harriman et al.[17] in which contour plots are presented showing the correlation between $\Lambda_{\overline{MS}}$ and η_g, for both BCDMS data[15] and EMC data,[18] augmented by

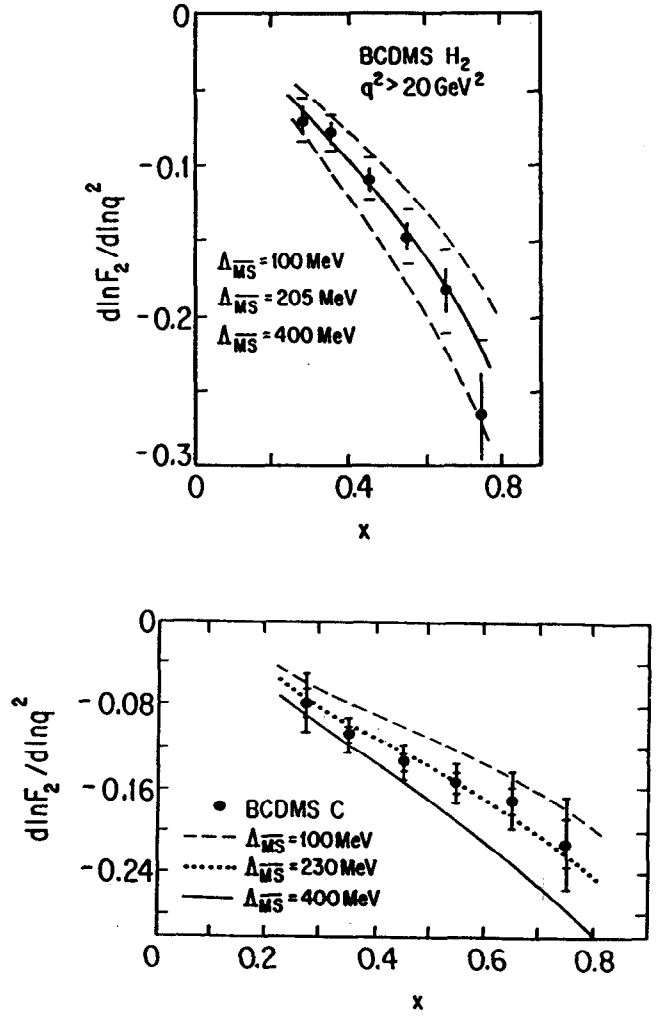

Figure 8: Non singlet analysis for large x done by the BCDMS collaboration[15] for deep inelastic muon scattering on both a carbon and hydrogen target.

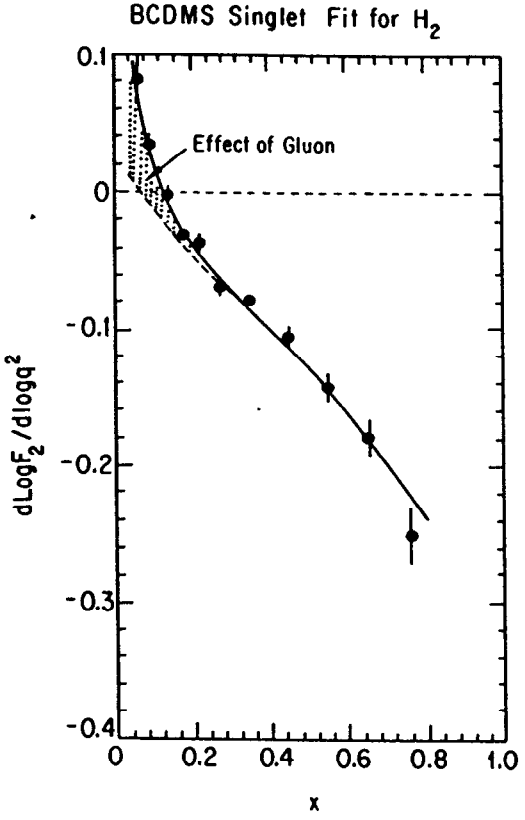

Figure 9: Variation of F_2^{em} with q^2 for all values of x obtained by the BCDMS collaboration for deep inelastic muon scattering on a Hydrogen target.[15]

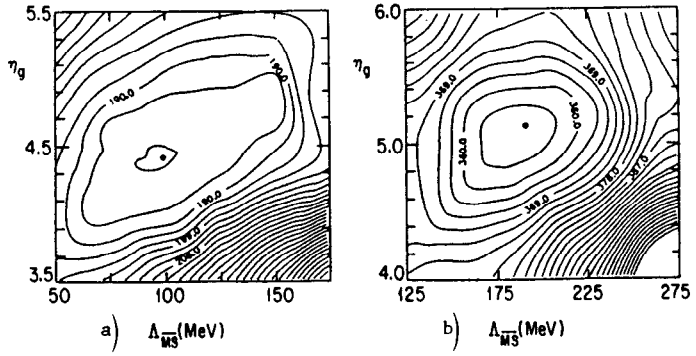

Figure 10: Correlation between $\Lambda_{\overline{MS}}$ and η_g for: a) EMC data; b) BCDMS data.[17]

neutrino deep inelastic and prompt photon[19] data. These plots are reproduced in Fig. 10. One sees that the EMC data prefers a smaller value for both η_g and $\Lambda_{\overline{MS}}$ [$\eta_g = 4.4; \Lambda_{\overline{MS}}\ (4) = 100 \pm 20\ MeV$] while the BCDMS data has larger values for both these quantities [$\eta_g = 5.1; \Lambda_{\overline{MS}}\ (4) = 190 \pm 20\ MeV$]. Part of this difference may be due to some experimental differences between the data sets.¶ However, it is clear from the figure that the uncertainty in the gluon distribution shape at q_0^2 introduces a corresponding variation in $\Lambda_{\overline{MS}}$. Thus, it would be particularly nice if one could obtain some independent information on $g(x;q^2)$. As we shall see in the next Section, this should be possible at HERA.

2. QCD Tests and the Gluon Distribution at HERA

The present, somewhat unsatisfactory, situation regarding QCD tests in deep inelastic scattering should be considerably improved at HERA. First of all, as can be appreciated from Fig. 11, at HERA there will be a substantial q^2 and x range accessible. Secondly, HERA affords the possibility to extract directly from data the gluon distribution $g(x;q^2)$ by a set of independent measurements. Even though the above two points make the experimental measurements which will be obtained at HERA very interesting, one cannot hide concomitant difficulties. For instance, although the large values of q^2 to be explored at HERA will lead to theoretical pristine data, since one can now really neglect higher twist corrections in the QCD tests, the electron proton cross section at large q^2 is small - scaling as $(q^2)^{-2}$ - and

¶These differences, however, appear to be resolved by the latest data obtained by the successor collaboration to EMC.[20]

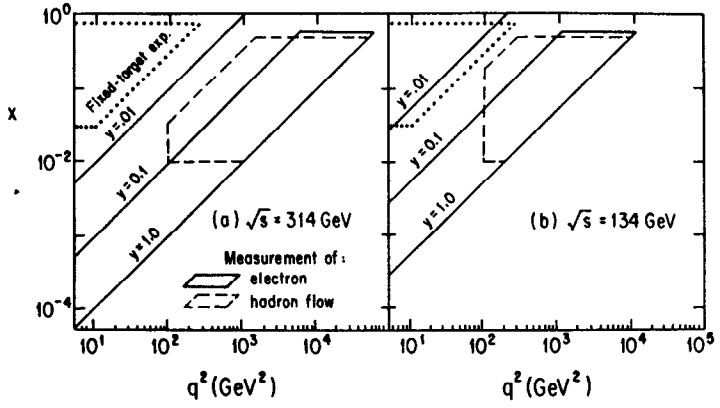

Figure 11: Kinematical range in the $x - q^2$ plane accessible at HERA.

one will be statistically limited. Furthermore, at large q^2, the logarithmic QCD variations one is looking for in the data are themselves small.

A few years ago Blümlein, Klein, Ingelman and Rückl (BKIR)[21] performed a phenomenological Monte Carlo analysis to ascertain how well one could test the scaling violations predicted by QCD at HERA. The result of their analysis was that of all structure functions accessible at HERA, only for F_2^{em} could one perform adequate QCD tests. Furthermore, because of the x-range probed, a singlet analysis is required in this case. Both of these statements are easily understood if one considers the number of events expected for $q^2 \geq 10 - 100\ GeV^2$. For an integrated luminosity $\int \mathcal{L}\ dt = 100\ pb^{-1}$, typical for a long run at HERA, only for the electromagnetic dominated processes $e^{\pm}p \to e^{\pm}X$ one expects over 10^4 events. These events, as can be seen from Fig. 11, are concentrated at x values below $x \leq 0.1$.

Because F_2^{em} has both singlet and non singlet pieces [c.f. Eq. (20)] the corresponding QCD analysis needs information on the gluon distribution. Let me rewrite Eq. (20) as

$$F_2^{em}(x;q^2) = \frac{1}{6}x\Delta(x;q^2) + \frac{5}{18}xF^s(x;q^2) \quad . \tag{36}$$

Then while the evolution with q^2 of the non singlet component $\Delta(x;q^2)$ is that of Eq. (13)

$$\frac{d\Delta(x;q^2)}{d\ \ell nq^2} = \frac{\alpha_s(q^2)}{2\pi}\int_x^1 P_{qq}(\frac{x}{\xi})\Delta(\xi;q^2) \quad , \tag{37}$$

the evolution of $F^s(x;q^2)$ is coupled to the evolution of the gluon distribution function $g(x;q^2)$. If f is the number of active flavors ($f = 4$ for HERA) then one has

$$\frac{d}{d\ \ell nq^2}F^s(x;q^2) = \frac{\alpha_s(q^2)}{2\pi}\int_x^1 \frac{d\xi}{\xi}\left[P_{qq}(\frac{x}{\xi})F^s(\xi;q^2) + 2fP_{qg}(\frac{x}{\xi})g(\xi;q^2)\right] \tag{38}$$

$$\frac{d}{d\ \ell nq^2}g(x;q^2) = \frac{\alpha_s(q^2)}{2\pi}\int_x^1 \frac{d\xi}{\xi}\left[P_{gg}(\frac{x}{\xi})g(\xi;q^2) + P_{gq}(\frac{x}{\xi})F^s(\xi;q^2)\right] \tag{39}$$

Three fits were done in the BKIR phenomenological analysis:

i.) A non singlet fit, which by necessity required that one restricted oneself to $x \geq 0.25$. Because of this restriction, the fit was statistically very poor.

ii.) A global fit of Δ, F^s and the gluon distribution g. This fit was dominated by the uncertainty in the input for this latter distribution.

iii.) A fit of Δ, F^s and g in which one assumes that the input gluon distribution $g(x;q_0^2)$ is known. This fit gave, by far, the best results.

Table 1: Results of the Monte Carlo fits of BKIR for HERA

Fit	$\delta\Lambda\ (MeV)$	$< q^2 >\ (GeV^2)$
Non singlet	± 176	2800
Δ, F^s, g	± 135	400
Fixed input glue	± 25	400

The results of these three fits are detailed in Table 1. ‖

It is easy to understand why the fit with a given input glue distribution, $g(x;q_0^2)$, gives so much better results by looking at the various contributions to the q^2 evolution of F_2^{em}. As can be seen from Fig. 12, for x below about 0.1 the gluon contribution fully dominates. I should note that the results of the fit with a fixed input glue distribution quoted in Table 1 came from a fit in which only data for $x > 0.01$ was included. As I shall discuss in much more detail later on, for x values below this value there are other effects which alter the Altarelli Parisi equations. Including these additional contributions would allow one to probe even lower x values, which become accessible at HERA, and would further improve the results on $\delta\Lambda$. It is clear, at any rate, that if one really wants to perform meaningful QCD tests at HERA, it is important that one be able to measure the input gluon distribution, $g(x;q_0^2)$, independently, since this function is a key to the QCD tests.

‖BKIR for simplicty only used lowest order QCD formulas, so that the Λ parameter, whose error is quoted in Table 1, is not $\Lambda_{\overline{MS}}(4)$. Nevertheless, one expects that $\delta\Lambda \simeq \delta\Lambda_{\overline{MS}}$.

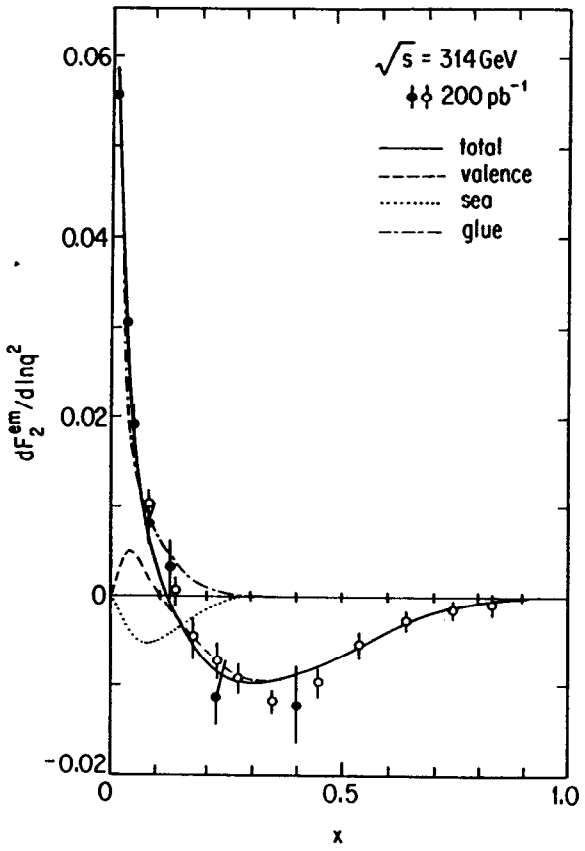

Figure 12: Contributions to the variation of F_2^{em} with q^2 at different x values.[21]

At HERA three ways have been suggested to obtain a direct measurement of the gluon distribution:

i) One may be able to extract $g(x;q^2)$ from a measurement of the longitudinal distribution $F_L(x;q^2)$.

ii) $g(x;q^2)$ can be obtained, in principle, through a study of inelastic ψ photoproduction: $\gamma p \to \psi X$.

iii) One may be able to determine $g(x;q^2)$ from inclusive charm and b quark production.

In what follows, I will make a few theoretical and phenomenological comments on each of the above methods for extracting $g(x;q^2)$.

2.1. F_L Measurement

Neglecting the contribution from Z exchange, the cross section for deep inelastic $e^{\pm}p$ scattering reads

$$\frac{d^2\sigma}{dxdq^2} = \frac{4\pi\alpha^2}{x(q^2)^2}\left\{\frac{[1+(1-y)^2]}{2}2xF_1(x;q^2) + (1-y)F_L(x;q^2)\right\} \quad , \tag{40}$$

where the longitudinal structure function $F_L(x;q^2)$ is given by

$$F_L(x;q^2) = F_2(x;q^2) - 2xF_1(x;q^2) \quad . \tag{41}$$

In the parton model (0^{th}order QCD) F_L vanishes identically because of the Callan Gross relation[22]:

$$F_2(x;q^2) = 2xF_1(x;q^2) \quad . \tag{42}$$

The Callan Gross relation follows as a simple kinematical result, if the scattering of the electrons (or positrons) is done on spin 1/2 partons.

In higher order in α_s, the partons which interact with the virtual photon exchanged now no longer encompass just quarks and antiquarks, but also include the spin 1 gluons. Thus one expects violations of the Callan Gross relation in QCD at non trivial order in α_s. Indeed, to leading order in α_s,[23] one finds that the longitudinal structure function F_L is given by

$$F_L(x;q^2) = \frac{\alpha_s(q^2)}{4\pi}\left\{4c_F\int_x^1\frac{d\xi}{\xi}(\frac{x}{\xi})^2F_2(\xi;q^2) + \sum_i e_i^2\int_x^1\frac{d\xi}{\xi}(\frac{x}{\xi})^2(1-\frac{x}{\xi})\xi g(\xi;q^2)\right\} \quad . \tag{43}$$

Hence $F_L(x;q^2)$ contains indirectly some information on the gluon distribution function.

Martin, Roberts and Stirling[24] made the important observation that, because x is very small in the experiments to be done at HERA, one can well approximate the integrals occuring in (43) by the actual values for F_2 and g at some fixed multiple of x. That is, one can approximate the integrals by their lower limit. Thus, for example, **

$$\int_x^1 \frac{d\xi}{\xi}(\frac{x}{\xi})^2 F_2(\xi;q^2) \simeq \frac{1}{2}F_2(0;q^2) + xF_2'(0;q^2) \simeq \frac{1}{2}F_2(2x;q^2) \ . \qquad (44)$$

and

$$\int_x^1 \frac{d\xi}{\xi}(\frac{x}{\xi})^2(1-\frac{x}{\xi})G(\xi;q^2) \simeq \frac{1}{6}G(0;q^2) + \frac{x}{2}G'(0;q^2) \simeq \frac{1}{6}G(3x;q^2) \ . \qquad (45)$$

Using the above and $c_F = 4/3$ and $\sum_i e_i^2 = \frac{10}{9}$, one arrives at an approximate formula for $xg(x;q^2) \equiv G(x;q^2)$:

$$xg(x;q^2) \simeq \frac{9}{5}\left\{\frac{3\pi}{2\alpha_s(q^2)}F_L(\frac{x}{3};q^2) - F_2(\frac{2x}{3};q^2)\right\} \ . \qquad (46)$$

That is, one can deduce the gluon distribution at a given x value from a measurement of both F_L and F_2 at smaller values of x.

Because F_L is sizable at small x, the dominant contribution to $xg(x;q^2)$ will come from the contribution of the longitudinal structure function itself. One must make sure, however, that the q^2 value one is measuring $F_L(x;q^2)$ at is large enough, to avoid having higher twist effects spoil the simple QCD formula (43). Indeed, for the small q^2 values where F_L is measured at SLAC ($q^2 \simeq 5\ GeV^2$) there appear to be substantial higher twist effects,[25] with the QCD and higher twist terms being comparable in magnitude:

$$[F_L(x;q^2)]_{\rm exp} = F_L^{QCD}(x;q^2) + \frac{8\kappa^2}{q^2}F_2(x;q^2) + .. \quad , \qquad (47)$$

with $\kappa^2 \simeq 0.05\ GeV^2$. At HERA, even for rather small x, q^2 values of the order of $50 - 100\ GeV^2$ are attainable, so higher twist effects should be substantially reduced.

To extract $g(x;q^2)$ one needs to separate $2xF_1(x;q^2)$ from $F_L(x;q^2)$, for fixed x and q^2. This requires doing measurements at different energies. This is clear, since the total energy squared $s = q^2/xy$, and to separate F_L from $2xF_1$ it is necessary to obtain the differential cross section (40) at different values of y. Cooper-Sarkar et al.[26] have investigated how well one can determine $xg(x;q^2)$ at HERA from measurements at $\sqrt{s} = 245\ GeV$ and $\sqrt{s} = 314\ GeV$, with a total integrated luminosity of 100 pb^{-1}. The results of this phenomenological analysis are shown in Fig. 13 for two values of q^2, big enough so as to avoid large higher twist contributions. The plots show the expected errors one will obtain at HERA, for two different types of gluon distributions. As can be seen from the figure the gluon distribution for rather small values of x ($3 \times 10^{-3} \lesssim x \lesssim 10^{-2}$) appears to be accessible and potentially well measured at HERA, independently of its detailed small x behaviour.

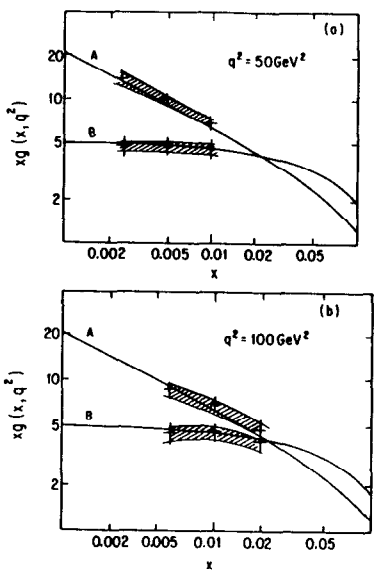

Figure 13: Errors expected to reconstruct two different gluon distributions at HERA from a measurement of $F_L(x;q^2)$.[26]

2.2. *Gluon Distribution from ψ* **Photoproduction**

The second method proposed to extract the gluon distribution function at HERA makes use of the fact that the ep collisions give rise to a very large high energy photoproduction cross section. For nearly real photons [$q^2 \simeq 0$] the ep cross section can be computed in the Weizsäcker-Williams approximation, in which the photoproduction cross section is convoluted with the probability of finding a photon in the incident electron

$$\sigma_{ep} = \frac{\alpha}{2\pi}\int dy P_{\gamma e}(y)\ \ell n\frac{q^2_{\rm max}}{q^2_{\rm min}}\ \sigma_{\gamma p}(E_\gamma = yE_e) \ . \qquad (48)$$

Note that $P_{\gamma e}$ is precisely the same splitting function as the quark-gluon splitting function P_{gq} of Eq. (16c), except that the weight factor here is $c_F = 1$ ††. Eq. (48)

**The analysis of[24] is slightly more sophisticated. However, the examples shown give the essence of the idea.

††Of course also $\alpha_s \to \alpha$ in Eq. (48).

makes it clear that HERA is an ideal place to study high energy photoproduction, with $s_{\gamma p} \simeq ys$.

Although high energy photoproduction is interesting per se, what is of most interest to study is heavy flavor production because, as is shown schematically in Fig. 14, this can occur through photon-gluon fusion. In principle, such a process provides a direct measurement of the gluon distribution function $g(x_g; Q^2)$. Here x_g is the fraction of momentum of the proton that the gluon carries, while Q^2 is a scale related to the production process. Obviously, before one can think of using heavy flavor photoproduction as a means of extracting information on the gluon distribution function, it is important to ascertain to what extent photon-gluon fusion dominates and to establish what is the relation of x_g and Q^2 to the scattering parameters.

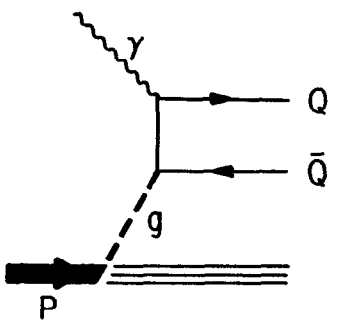

Figure 14: Schematic diagram illustrating heavy flavor production via photon-gluon fusion.

One possible way to isolate particular values of x_g (and Q^2), which has been suggested by Martin, Ng and Stirling,[27] is to look for photoproduction of ψ's. This process results again from photon gluon fusion, with the produced $c\bar{c}$ pairs binding into a ψ. Since the ψ is a color singlet, for this process to occur requires that an additional gluon be produced in association with the ψ, as shown schematically in Fig. 15. The scale Q^2 associated to the gluon distribution is related to the ψ mass and the transverse momentum $p_\perp$ of the produced ψ's. Whether one should take Q^2 to be simply $Q^2 = m_\psi^2$, or one should use $Q^2 = P_\perp^2 + m_\psi^2$, or instead some other intermediate value, cannot really be resolved without a higher order calculation. However, because the relevant transverse momentum of the produced ψ's is quite limited, there is not much difference between these two scales and the choice $Q^2 \simeq m_\psi^2$ seems a sensible first approximation[27]‡‡

‡‡I will return at the end of these lectures to the issue of scales in heavy flavor production.

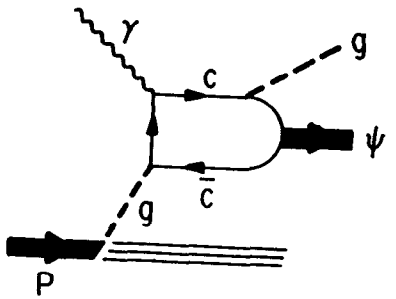

Figure 15: Diagram leading to ψ photoproduction.

The cross section for $\gamma p \to \psi x$ is dominated by values of the gluon momentum fraction x_g near its lower limit, $(x_g)_{\min} \simeq \frac{m_\psi^2}{s_{\gamma p}}$. The actual cross section depends on the knowledge of the wavefunction of the ψ at the origin, which enters to typify the binding of the produced $c\bar{c}$ pair to form a ψ. Fortunately, this wavefunction is known experimentally from the size of the leptonic width of the ψ. The analysis of Martin, Ng and Stirling[27] shows that the differential cross section for ψ photoproduction can be written as

$$\frac{d\sigma}{dx_g}(\gamma p \to \psi X) = x_g g(x_g; Q^2) \frac{\Gamma(\psi \to e^+e^-)}{m_\psi^3} K[x_g; \frac{s_{\gamma p}}{m_\psi^2}] \ . \qquad (49)$$

Here the function $K[x_g; \frac{s_{\gamma p}}{m_\psi^2}]$ is a known kinematic function which is sharply peaked near $x_g \simeq (x_g)_{\min}$. Using cuts of $p_\perp^2 > 0.1 m_\psi^2$ and $z = p_\psi \cdot P/q \cdot P < 0.8$, Martin, Ng and Stirling give an approximate handy formula for the integrated ψ photoproduction cross section which is directly proportional to the gluon distribution at some average effective value of x_g, near $(x_g)_{\min}$. They find, using $Q^2 \simeq m_\psi^2$,

$$\sigma(\gamma p \to \psi X) \simeq 1.5 \bar{x}_g g(\bar{x}_g; m_\psi^2)\ nb \qquad (50)$$

where $\bar{x}_g \simeq 3.4 m_\psi^2/s_{\gamma p} = 3.4\ m_\psi^2/ys$. Thus, using Eq. (48), one sees how ψ production at HERA, in principle, can be used to extract the gluon distribution in a restricted range in x and $q^2 [x \simeq 10^{-3}\ ;\ q^2 \simeq 10\ GeV^2]$:

$$\frac{d\sigma(ep \to \psi X)}{dy} \simeq \frac{1.5\alpha}{2\pi}\left[\frac{1+(1-y)^2}{y}\right] \bar{x}_g g(\bar{x}_g; m_\psi^2)\ \ell n \frac{q^2_{\max}}{q^2_{\min}} \ . \qquad (51)$$

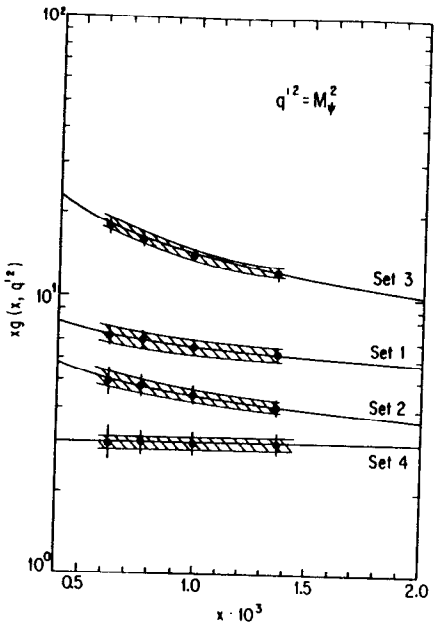

Figure 16: Errors expected to reconstruct various possible gluon distributions using ψ production in a 100 pb^{-1} HERA run.[28]

Fig. 16, taken from the phenomenological study of Tkaczyk, Stirling and Saxon,[28] shows how well one could determine $g(x; m_\psi^2)$ with ψ production in a 100 pb^{-1} HERA run.

Even though Fig. 16 is rather impressive, it is important to ask how reliable is this determination of $g(x; q^2)$. At least two issues need to be answered:

i.) Will all the ψ's which will be produced at HERA originate from photon gluon fusion?

ii) How trustworthy is the computation of ψ photoproduction from the diagram of Fig. 15?

Although not all the ψ's produced at HERA will originate from photon gluon fusion, studies by Kunszt and Sterling,[29] Fletcher, Halzen and Robinett[30] and Martin, Ng and Stirling[27] show that one can successfully isolate the ψ's produced from the process $\gamma g \to \psi X$ from all other produced ψ's. For instance, although there will be a substantial number of ψ's produced through radiative χ decay ($\chi \to \psi\gamma$), since χ production itself through gluon gluon fusion is expected to be large,[30] these "background" ψ's can be eliminated by an angular cut. As shown in Fig. 17, the ψ's produced from radiative χ decay are produced very much more along the proton direction and a cut of, say, $\cos\theta \lesssim 0.5$, should effectively eliminate this background. Because HERA will photoproduce an abundant number of B mesons, and the $B \to \psi X$ branching ratio is rather large, one must also worry about ψ's produced in this fashion. Fortunately, again kinematics can help. The ψ's coming from the decay of a B meson have much larger $p_\perp$'s, as is shown in Fig. 18. Thus a $p_\perp$ cut of a few GeV, say $p_\perp \lesssim 3\ GeV$, should eliminate most of these other unwanted ψ's.

For the second question above, however, the answer is not quite so sanguine. In fact, it is quite difficult to judge the theoretical reliability of the calculation of the process $\gamma g \to \psi g$ from Fig. 15. In effect, one needs really to compute the $0(\alpha_s)$ corrections to this process - a rather prohibitive task - before one can answer this question. However, perhaps one can gain some insight from the, diagramatically similar, decay process $\psi \to gg\gamma$. Unfortunately, this latter process is known to have large corrections in the $\overline{MS}$ scheme,[31] where one finds

$$\Gamma(\psi \to gg\gamma) = \Gamma_0\left\{1 - \frac{6.7}{\pi}\alpha_s(m_c^2)\right\} \quad . \tag{52}$$

Using $\alpha_s = 0.29 \pm 0.02$,[31] the higher order corrections reduce the rate for this process by more than a factor of 2. Whether the same thing obtains for the process $\gamma g \to \psi g$ is an open question, but the result (52) certainly should give one pause.

2.3. Determing the Gluon Distribution from Heavy Flavor Production

The gluon distribution function can also be determined at HERA by studying directly the production of heavy flavors. Both charm and bottom quarks will be abundantly produced at HERA, with the dominant mechanism being the photon gluon fusion shown in Fig. 14. Roughly speaking, the cross section for producing a $c\bar{c}$ pair through photon gluon fusion is near 1 μb, while $b\bar{b}$ production is about 10 nb. The heavy quarks are produced with a rather flat rapidity distribution and a $p_\perp$ spectrum which has a much broader tail for b quarks than for c quarks[32,33].

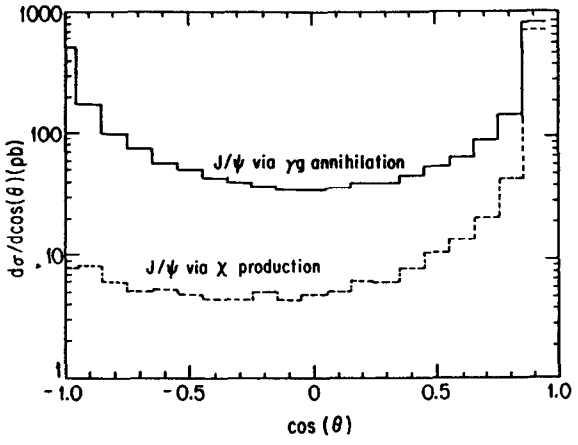

Figure 17: Polar angle distribution of ψ's produced via photon gluon fusion and through radiative χ decays. [29]

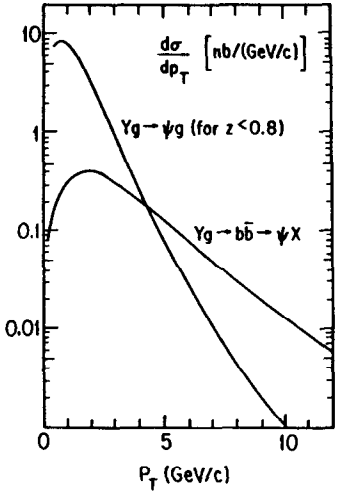

Figure 18: The $p_\perp$ dependence of ψ's produced via photon gluon fusion and from B decay at HERA. [27]

The cross section for $Q\bar{Q}$ production - where Q is a heavy quark - at HERA can be obtained from the analogous photoproduction cross section by using the Weiszäcker Williams formula, Eq. (48). In lowest order in QCD, the photoproduction cross section is proportional to the gluon distribution function $g(x_g;Q^2)$, and one finds[33]

$$\frac{d\sigma(\gamma p \to Q\bar{Q}X)}{dx_g} = g(x_g;Q^2)\left[2\pi\frac{\alpha\alpha_s}{\hat{s}}e_Q^2\right]\cdot\left\{(1+w-w^2)\,\ell n\frac{1+\chi}{1-\chi}-\chi(1+w)\right\} \ . \quad (53)$$

Here $\hat{s}$ is the invariant mass squared of the $Q\bar{Q}$ pair, while $w = 4m_Q^2/\hat{s}$ and $\chi = [1-w]^{1/2}$ are related to the velocity of the heavy quark. Note that the gluon's momentum fraction is directly related to the invariant mass of the $Q\bar{Q}$ pair

$$x_g = \frac{\hat{s}}{ys} \ . \quad (54)$$

To be able to use the above formula to determine the gluon distribution function one needs to know what scale Q^2 one should take and, further, what scale is relevant for α_s in Eq. (53). As I alluded to earlier, and will explain in more detail towards the end of these lectures, one cannot really determine what Q^2 to use, or what $\alpha_s(\mu^2)$ to take, until higher order corrections of $0(\alpha\alpha_s^2)$ are computed. Ellis and Kunszt,[32] on the basis of a partial calculation of the higher order corrections, noted that the product $g(x_g;Q^2)\alpha_s(\mu^2)$, which enters in Eq. (53), has compensating tendencies if one takes $Q^2 \sim \mu^2$. As Q^2 decreases the gluon distribution, at fixed x_g, also tends to decrease, while the opposite is the case for $\alpha_s(\mu^2)$. From their analysis, Ellis and Kunszt[32] suggested that a sensible choice to take for these scales is

$$Q^2 = \mu^2 = p_\perp^2 + m_Q^2 \ . \quad (55)$$

This choice remains reasonable also in the light of the full $0(\alpha\alpha_s^2)$ calculation of the process $\gamma g \to Q\bar{Q}(g)$ which has now been completed by Ellis and Nason.[34] However, a theoretically more consistent approach incorporates these corrections directly in a transverse momentum convolution rather than just as some overall effective momentum scale.[35] I will return to give a fuller explanation of this point at the end of the next Section.

Besides the question of which scales enter in Eq. (53), a crucial other issue is how one determines experimentally x_g or, equivalently, the $Q\bar{Q}$ invariant mass. Here a nice trick has been suggested by Schuler and collaborators.[36] In the case of photoproduction, the HERA lab frame in which the electron and proton collide head on, and the $Q\bar{Q}$ CM frame are just related by a boost. Thus the corresponding rapidities add, and one finds[36]

$$y_{\rm HERA} = y_{Q\bar{Q}CM} + \frac{1}{2}\,\ell n\left[\frac{yE_e}{x_g E_p}\right] \ , \quad (56)$$

where E_e, E_p are the energies of the electron and protons in the HERA frame. If one studies the heavy quark production through the subsequent leptons produced in the heavy quark decay, i.e.,$ep \to eQ\bar{Q}X \to e\ell^+\ell^- X$, then one expects that in the $Q\bar{Q}$ CM frame the $\ell^+\ell^-$ rapidity vanishes. If $y(\ell^+\ell^-)_{Q\bar{Q}CM} = 0$, by measuring the $\ell^+\ell^-$ rapidity in the HERA lab frame one reconstructs directly x_g. Using Eq. (56), it follows that

$$x_g = \frac{yE_e}{E_p} exp - \left\{ 2y(\ell^+\ell^-)_{Q\bar{Q}CM} \right\} . \qquad (57)$$

Fig. 19 shows the result of a phenomenological study of this procedure for the proposed ep collider that would result from colliding LEP electrons with the protons of the LHC. In this Monte Carlo study, Eq. (57) was used to determine x_g and the figure shows how well the reconstructed gluon distribution compares to the input gluon distribution. It is clear that the method appears to work very well. Thus, if the theoretical underpinnings related to higher order QCD corrections to Eq. (53) can be successfully handled, it appears that heavy flavors production in ep collisions can provide a very good independent determination of the gluon distribution function.

3. Deep Inelastic Scattering at Small x

Besides trying to measure in an independent manner the gluon distribution function, HERA will naturally explore deep inelastic scattering at extremely low values of x [c.f. Fig. 11 where the $x - q^2$ range which can be accessed at HERA is detailed]. This is an extremely interesting region theoretically. Furthermore, predictions for high energy experiments at the SSC and LHC will depend considerably on our knowledge of the structure functions of quarks and, particularly, of gluons at small x. Thus it behooves us to spend the rest of these lectures discussing what are the theoretical expectations and what are the uncertainties, concerning deep inelastic scattering in this region.

What makes the small x region in deep inelastic scattering interesting is that new dangerous logarithms, involving $\alpha_s\, \ell nx$ enter. Through the Altarelli Parisi equations and factorization we learned in Sec. 2 how to handle the large infrared logarithms that threatened perturbative QCD. For small x physics we have to understand what to do with these new $\alpha_s\, \ell nx$ terms. In fact, as Levin and Ryskin have emphasized,[38] there are 3 interesting regions to explore in the $x - q^2$ plane. These are depicted schematically in Fig. 20. These are:

i) The purely deep inelastic region, where q^2 is large ($q^2 >> q_0^2$) and x is moderate ($x \gtrsim x_0$).

ii) The deep inelastic, small x region, where q^2 is large ($q^2 >> q_0^2$) but x is small ($x << x_0$) .

iii) The Regge region, where both q^2 and x are small ($q^2 \lesssim q_0^2$; $x << x_0$) .

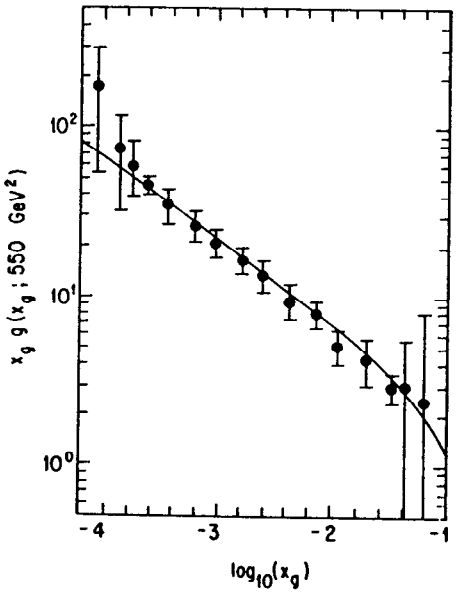

Figure 19: Comparison of the reconstructed gluon distribution, obtained by studying the dileptons produced in heavy quark decays, compared to an assumed input gluon distribution. [37]

Although it is difficult to draw strict boundaries between the regions, sensible choices for q_0^2 and x_0 are $q_0^2 \simeq 4\ GeV^2$, $x_0 \simeq 10^{-2}$.

In the deep inelastic region the only important large logarithms involve $\alpha_s\, \ell nq^2$ and their proper handling eventually leads to the running of the parton distribution functions. How these functions run is detailed by the Altarelli Parisi equations. In the small x, deep inelastic region, one has both $\alpha_s\, \ell nx$ and $\alpha_s\, \ell nq^2$ terms, along with double logarithms like $\alpha_s\, \ell nx\, \ell nq^2$. These logarithms, as we shall see, if left unchecked give rise to unphysical characteristics. However, when parton-parton interactions at low x values are included through the, so called, Gribov Levin Ryskin (GLR) equation,[39] one again can control these dangerous logarithms. The GLR equation will also help tame some of the difficulties caused by the $\alpha_s\, \ell nx$ logarithms, which enter in the Regge region. Although there has been considerable theoretical work in the low x region, the status of the theory here is considerably less well established than in the purely deep inelastic region.

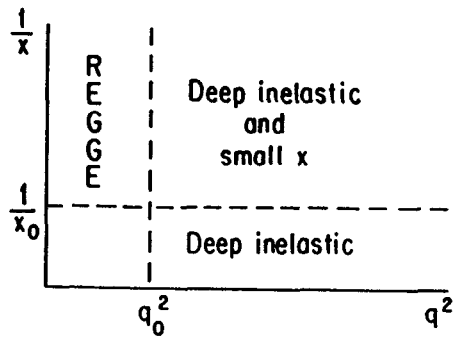

Figure 20: Interesting regimes in the $x - q^2$ plane.[38]

To begin to understand some of the new elements involved in low x physics, it is useful to return to examine the Altarelli Parisi equations. Recall that the Altarelli Parisi equation for the moments of the non singlet structure function

$$\frac{dM_n(q^2)}{d\,\ell nq^2} = \frac{\alpha_s(q^2)}{2\pi}\, A_n M_n(q^2) \ , \tag{58}$$

where

$$M_n(q^2) = \int_0^1 \frac{d\xi}{\xi}\xi^n f^{NS}(\xi;q^2) \tag{59}$$

and

$$A_n(q^2) = \int_0^1 \frac{d\xi}{\xi}\xi^n P_{qq}(\xi) \ , \tag{60}$$

had a very simple solution [c.f. Eq. (26)]:

$$M_n(q^2) = C_n[\ \ell n\frac{q^2}{\Lambda^2}]^{\frac{A_n}{2\pi b}} \tag{61}$$

It is useful to rewrite Eq. (61) in terms of a power series expansion. By doing so one can associate each term in the expansion with specific Feynman diagrams, whose set when summed gives the full moments of the non singlet distribution function.[40] Expanding Eq. (61) one has

$$\begin{aligned} M_n(q^2) &= C_n\, exp\{\frac{A_n}{2\pi b}\ \ell n\ \ell nq^2/\Lambda^2\} \\ &= C_n \sum_h \frac{1}{h!}[\frac{A_n}{2\pi b}\ \ell n\ \ell nq^2/\Lambda^2]^h \ . \end{aligned} \tag{62}$$

This formula can also be derived from a diagrammatic analysis of specific Feynman graphs which contribute to the non singlet structure functions - and

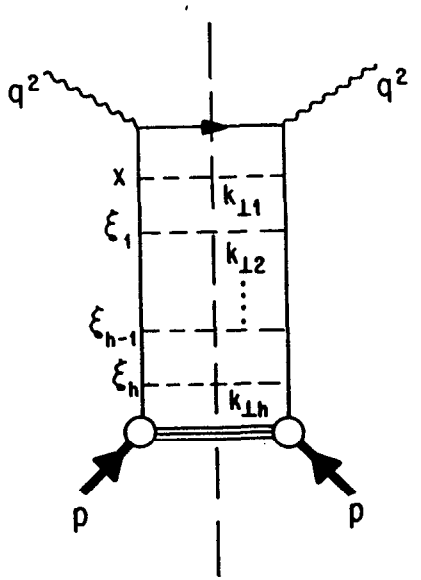

Figure 21: Ladder graph whose discontinuity in the axial gauge contributes to the h^{th} term in Eq. (62). In this diagram the gluon transverse momenta are ordered $(q^2 >> k_{\perp 1}^2 \ldots >> k_{\perp h}^2)$ as are the momentum fractions carried by the quarks $\xi_h > \xi_{h-1} > \ldots > \xi_1$.

hence to their moments. Because one is only interested in the leading logarithmic behaviour, one can simplify both the structure of the terms one keeps and their associated phase space factors. Effectively, one retains in these diagrams only those pieces in which the momenta of the produced partons are ordered in a particular way.[41] I claim, without particular justification at this moment, that the h^{th}- term of Eq. (62) can be associated with the absorptive part* of the diagram in Fig. 21 containing h gluon rungs. Indeed, it is easy to check that one can reproduce the formula (62), if one assumes furthermore that the transverse momenta of the gluons are ordered, so that the gluons farther away from the incoming virtual vector boson have smaller transverse momenta. That is, $q^2 > k_{\perp 1}^2 > k_{\perp 2} \ldots > k_{\perp h}^2$. In addition, to reproduce Eq. (62), the longitudinal momentum fraction of the quarks in between the emitted gluons must also have decreasing value, as the quarks get progressively farther and farther away from the incident proton. That is, $\xi_h > \xi_{h-1} \ldots > \xi_1 > x$. The result for $M_n(q^2)$ is recovered if the contribution

*That structure functions are associated with absorptive parts of Feynman diagrams is particularly clear in a parton picture, since in calculating the deep inelastic cross section one sums over incoherent parton production processes.

of the qqg vertex to the absorptive part of the non singlet structure function, in this specified kinematical ordering, is simply given by

$$V(\xi_{h-1}, \xi_h; k_{\perp h}) = \frac{\alpha_s(k^2_{\perp h})}{2\pi} \cdot \frac{1}{k^2_{\perp h}} P_{qq}(\frac{\xi_{h-1}}{\xi_h}) \quad . \tag{63}$$

The vertex associated with Eq. (63) is shown in Fig. 22 .

To obtain the contribution of graphs of the type shown in Fig. 21 to the non singlet structure function, one must perform the phase space integrals for the h-rung gluon diagram with the restrictions indicated, and then sum over the number of produced gluons from $h = 1$ to $h = \infty$. Let us check that indeed the h-rung term precisely gives the right contribution to Eq. (62). The contribution to the non-singlet structure function is

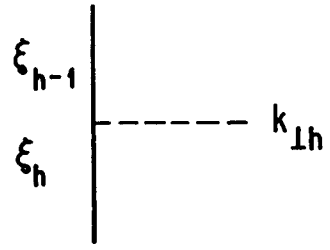

Figure 22: The qqg vertex of Eq. (63), with the corresponding kinematics shown.

$$[F^{NS}(x;q^2)]_{h-rung} = \int^{q^2} \frac{dk^2_{\perp 1}}{k_{\perp 1}} \frac{\alpha_s(k^2_{\perp 1})}{2\pi} \int_x^1 \frac{d\xi_1}{\xi_1} P_{qq}(\frac{x}{\xi_1}) \cdots \int^{k^2_{\perp h-1}} \frac{dk^2_{\perp h}}{k^2_{\perp h}} \frac{\alpha_s(k^2_{\perp h})}{2\pi} \int_{\xi_{h-1}}^1 \frac{d\xi_h}{\xi_h} P_{qq}(\frac{\xi_{h-1}}{\xi_h}) f^{NS}(\xi_h) \tag{64}$$

where $f(\xi)$ is the parton distribution of the initial quark in Fig. 21. In this language it is the emission of the $h-$gluons - with h going from 1 to ∞ - which makes the structure function $F^{NS}(x;q^2)$ run.† Taking the moments of Eq. (64) gives for the h-rung contribution of $M_n(q^2)$ the following expression:

$$[M_n(q^2)]_{h-rung} = \int_0^1 \frac{d\xi_h}{\xi_h} \xi_h^n f^{NS}(\xi_h) [\frac{A_n}{2\pi}]^h \cdot \{\int^{q^2} \frac{dk^2_{\perp 1}}{k^2_{\perp 1}} \alpha_s(k^2_{\perp 1}) \cdots \int^{k^2_{\perp h-1}} \frac{dk^2_{\perp h}}{k^2_{\perp h}} \alpha_s(k^2_{\perp h})\} \quad . \tag{65}$$

Using that $\alpha_s(k^2_\perp) = 1/b\ \ell n(k^2_\perp/\Lambda^2)$ it is easy to check that the nested integrals in the curly bracket in Eq. (65) just give

$$\{Eq.\ (65)\} = \frac{1}{h!}(\frac{1}{b} \ell n\ \ell n\ q^2/\Lambda^2)^h \quad . \tag{66}$$

Hence, indeed Eq. (65) reproduces the h^{th} term of Eq. (62), provided one identifies the coefficient C_n as the n^{th} moment of the "fixed momentum" parton non singlet distribution:

$$C_n = \int_0^1 \frac{d\xi_h}{\xi_h} \xi_h^n f^{NS}(\xi_h) \quad . \tag{67}$$

Several comments are in order:

i) We have demonstrated that the contribution to the non singlet structure function due to the h-rung gluon graph of Fig. 21, with the kinematics as we specified and with the qqg vertex of Eq. (63), reproduces precisely the h^{th} term of Eq. (62). This equivalence of the Altarelli Parisi equations with ordered **ladder graphs**, with vertices given by the splitting functions of Eq. (63), actually holds only in an axial gauge.[41] In any other gauge, the most singular contribution to the structure function arises not only from diagrams in which the gluons are emitted from the initial partonic leg, but also from graphs where the gluons are emitted from the final partons. Of course, since the structure functions are gauge invariant, the answer one computes is gauge independent. Obviously, however, it is physically much more intuitive to present the calculation in an axial gauge, where the only diagrams which give logarithmic enhancements of ℓnq^2, reflecting the collinear singularities caused by gluon emission, are the ladder diagrams of Fig. 21.

ii) It is clear, either from Eq. (62) or from computing the ladder diagrams of Fig. 21, that the Altarelli Parisi equations in leading order in QCD just give the leading logarithmic contributions. That is, the Altarelli Parisi equations sum up all contribution of order $(\alpha_s\ \ell nq^2/\Lambda^2)^h$ in graphs with h-rungs, yielding

†Note that, in this effectively "lowest order" treatment, the hadronic structure function $F^{NS}(x;q^2)$ coincides with the partonic non singlet distribution function $f^{NS}(x;q^2)$.

a factor of $(\ell n q^2/\Lambda^2)^h$. Because $\alpha_s \ell n q^2/\Lambda^2 \sim 0(1)$, such a sum is necessary and the Altarelli Parisi equations just give one the results of such a leading logarithm sum.

This reinterpretation of the Altarelli Parisi equations in terms of ladder diagrams sums is very useful for understanding what happens at low x. In the low x region, one encounters new logarithmic effects associated with $\ell n x$, or more precisely, with $\ell n\ 1/x$. In the Regge region, as we shall see, it will be important to sum up all terms of $0([\alpha_s\ \ell n\ 1/x]^h)$, while in the low x, deep inelastic region one will need to account for, in addition, of all terms containing $(\alpha_s\ \ell n\ q^2)^h$, as well as mixed terms like $(\alpha_s\ \ell n\ q^2\ \ell n\ 1/x)^h$. Because q^2 and x are different kinematical parameters and α_s depends only on q^2, $\alpha_s(q^2) \sim (\ell n q^2)^{-1}$, it is clear that in both regions one will obtain progressively worse behaved terms as $x \to 0$. Thus, unless one includes some more physical input in this region, it is not surprising that one eventually runs into trouble.

To begin to appreciate the problems one encounters, it is useful to start by looking at the Altarelli Parisi equations in the low x limit. Although we know that these equations sum up correctly all the $\ell n\ q^2$ terms, they do not account completely for all the small x physics. This physics, as we have just argued, can generate further logarithms of $\ell n 1/x$ which need not be contained in the ladder graphs of Fig. 21. Because the gluon distribution $g(x;q^2)$ dominates over the quark distributions at small x [c.f. Fig. 12], it is sensible to just retain this distribution function in the Altarelli Parisi equations. That is, let us consider Eq. (39) in which, however, we drop altogether the singlet contribution due to $f^S(\xi;q^2)$. In addition, since we are interested in the limit as $x \to 0$, we can retain in the gluon-gluon splitting function only the leading term as $z = \frac{x}{\xi} \to 0$, namely

$$P_{gg}(\frac{x}{\xi}) \simeq 2c_A \frac{\xi}{x} \quad . \tag{68}$$

Thus, in the low x - limit, the Altarelli Parisi equation we want to examine just reduces to the following equation for the gluon distribution function:

$$\frac{d}{d\ \ell n\ q^2}[xg(x;q^2)] = \int_x^1 \frac{d\xi}{\xi} \frac{c_A \alpha_s(q^2)}{\pi} [\xi g(\xi;q^2)] \quad . \tag{69}$$

Eq. (69) can actually be rather readily solved, if one assumes sufficiently simple boundary conditions. For these purposes, following Gribov, Levin and Ryskin,[39] it is useful to change variables from x and q^2 to z and σ, where

$$z = \frac{c_A}{\pi b}\ \ell n\ \frac{1}{x}; \quad \sigma = \ell n\ \ell n q^2/\Lambda^2 \quad . \tag{70}$$

Then, defining $G(z;\sigma) = xg(x;q^2)$, it is easy to see that G obeys the integro-differential equation

$$\frac{\partial G(z;\sigma)}{\partial \sigma} = \int_0^z dz' G(z';\sigma) \quad . \tag{71}$$

If one takes as a boundary condition that at $\sigma = \sigma_0$ $G(z;\sigma_0) = 1$, then it is easy to show[39] that the solution of Eq. (71) is precisely given by a modified Bessel function of imaginary argument:

$$G(z;\sigma) = I_0[\sqrt{4z(\sigma - \sigma_0)}] \quad . \tag{72}$$

We will be interested particularly in the small x case where $z\sigma >> 1$. In this case Eq. (72) just gives that $G(z,\sigma) \sim \exp 2[z\sigma]^{1/2}$, so that in the small x limit the gluon distribution function takes the form

$$xg(x;q^2)\ \underset{x \to 0}{\sim}\ \exp 2[\frac{c_A}{\pi b}\ \ell n\ \frac{1}{x} \ell n\ \ell n\ q^2/\Lambda^2]^{1/2}. \tag{73}$$

As we shall see, this result is precisely that which arises from summing a series of double logarithms involving terms of $0\Big([\alpha_s\ \ell n \frac{1}{x}\ \ell n\ \ell n \frac{q^2}{\Lambda^2}]^h\Big)$.

The result (73) is obtained again by summing the discontinuities of a set of ladder graphs quite similar to those of Fig. 21, but where now all rungs are gluons except for a final quark-antiquark pair where the external currents V^* attach themselves. The relevant h-rung graph is shown in Fig. 23. In this graph, to reproduce Eq. (73) one must assume that besides the transverse momentum ordering of the emitted gluons, $q^2 >> k_{\perp 1}^2 >> \ldots >> k_{\perp h}$, these excitations have also a longitudinal ordering in which the rung closest to the external current has the least longitudinal momentum fraction: $x << x_1 << \ldots << x_h$. Finally, the triple gluon vertex reflects the form of the gluon gluon splitting function (68)‡:

$$V_{3g}(i) = \frac{c_A}{\pi} \frac{\alpha_s(k_{\perp i}^2)}{k_{\perp i}^2} = \frac{c_A}{\pi b\ \ell n\ k_{\perp i}^2/\Lambda^2} \frac{1}{k_{\perp i}^2} \quad . \tag{74}$$

Using the vertex (74) and the ordered phase space described above, the contribution of the h-rung ladder or Fig. 23 to $xg(x;q^2)$ is

$$\begin{aligned}[xg(x;q^2)]_{h-rung} \;=\; \{ & \int^{q^2} \frac{dk_{\perp 1}^2}{k_{\perp 1}^2} \frac{1}{\ell n k_{\perp 1}^2/\Lambda^2} \int_x \frac{dx_1}{x_1} \frac{c_A}{\pi b} \cdots \\ & \int^{k_{\perp h-1}^2} \frac{dk_{\perp h}^2}{k_{\perp h}^2} \frac{1}{\ell n k_{\perp h}^2/\Lambda^2} \int_{x_{h-1}} \frac{dx_h}{x_h} \frac{c_A}{\pi b} \} \quad . \end{aligned} \tag{75}$$

‡The factor of x/ξ is absorbed into the phase space factor.

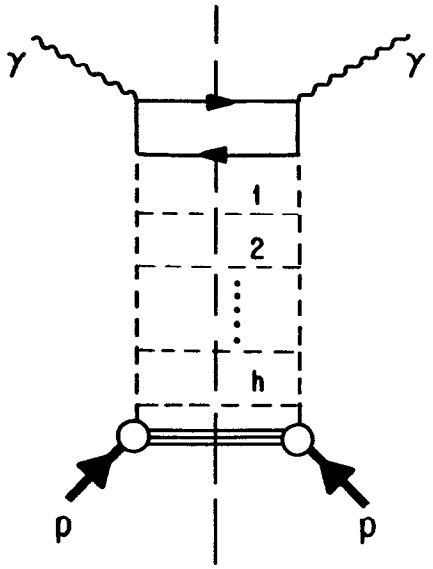

Figure 23: Ladder graphs whose discontinuity produces the gluon distribution function given in Eq. (73), when one uses the gluon vertices of Eq. (74) and a phase space which is ordered in both longitudinal and transverse momentum.

The integrals within the curly bracket above contain two kinds of nested integrals. The transverse momentum nested integrals will give as before a factor of [cf Eq. (66)]

$$\text{Transverse nested integrals } = \frac{1}{h!}(\ell n\ \ell n q^2/\Lambda^2)^h. \tag{76}$$

The longitudinal nested integrals, on the other hand, will give a factor of

$$\text{Longitudinal nested integrals} = \frac{1}{h!}[\frac{c_A}{\pi b}\ \ell n\frac{1}{x}]^h \ . \tag{77}$$

Thus the sum over h of the h-rung integrals of Fig. 23 gives for the gluon structure function

$$xg(x;q^2) = \sum_h \frac{1}{(h!)^2}[\frac{c_A}{\pi}\ \ell n\frac{1}{x}\ \ell n\ell n\frac{q^2}{\Lambda^2}]^h \ . \tag{78}$$

As anticipated, this is indeed a sum of double logarithms in $\alpha_s\ \ell n\frac{1}{x}\ \ell n q^2$. This sum, in fact, can be performed and gives precisely the Bessel function I_0 encountered previously:

$$xg(x;q^2) = I_0[2(\frac{c_A}{\pi b}\ \ell n\frac{1}{x}\ \ell n\ \ell n q^2/\Lambda^2)^{1/2}] \simeq\ exp\ 2[\frac{c_A}{\pi b}\ \ell n\frac{1}{x}\ \ell n\ \ell n q^2/\Lambda^2]^{1/2} \ , \tag{79}$$

which establishes our contention.

The result of Eq. (79), however, **cannot** be correct as $x \to 0$, since it leads to a violation of unitarity! It is easy to check that Eq. (79) as $x \to 0$ grows faster than any power of (ℓns). But we know that unitarity restricts the ep cross section to grow at most as $(\ell ns)^2$ since:

$$\sigma_{ep}\ \sim \frac{\alpha\alpha_s}{q^2} xg(x;q^2) \leq \sigma_{pp} \leq \text{const}\ (\ell ns)^2 \quad , \tag{80}$$

where the second inequality is the famous Froissart[42] bound. Hence, it follows that the Altarelli Parisi evolution equations do not give a complete description of the problem for small x and must be suitably modified.

Before discussing this modification, it is useful to consider also the expectation in the Regge region ($q^2 \leq q_0^2,\ x << x_0$) for very small x. As we shall see, also here similar problems with unitarity are encountered. The appropriate equation to describe the behaviour of the structure functions in the Regge region was first discussed by Lipatov[43] and then derived and discussed in more detail by Balitsky, Fadin, Kuraev and Lipatov in a series of papers.[44] This equation - the BFKL equation - again can be obtained by looking at the sum of ladder graphs containing gluonic rungs shown in Fig. 23. However, in contrast to what happens for the small x deep inelastic region, because q^2 is not large, the gluon rungs will only have longitudinal ordering ($x << x_1 \ldots << x_h$) but no transverse ordering. Because of this, furthermore, the three gluon vertex which enters in the ladder graph sum, in contrast to the vertex of Eq. (74), now depends on both $k^2_{\perp i-1}$ and $k^2_{\perp i}$. The idea that, in the Regge region, deep inelastic scattering is dominated by only longitudinally ordered ladder graphs gives an explicit realization of the Pomeron for these processes and was first formulated by Lipatov.[43] It embodies the suggestion of Low and Nussinov[45] that the Pomeron can be represented as a t - channel 2 gluon exchange process.

The BFKL equation is more complicated than the corresponding Altarelli Parisi equation since there is no transverse ordering and the three gluon vertex has a non trivial dependence on both $k^2_{\perp h-1}$ and $k^2_{\perp h}$. As a result, I will content myself to examine only the structrue of its h-rung factor, rather than the whole equation. Because in the ladder graphs of Fig. 23 the longitudinal integrals are nested, the BFKL equation will also have for the h-rung contribution a factor of $\frac{1}{h!}(\ell n\frac{1}{x})^h$. However, the transverse momentum dependence in the BFKL case is more complex. One finds for the h-rung contribution to the gluon structure function the expression

$$[xg(x;q^2)]^{BFKL}_{h-rung} = \frac{1}{h!}(\ell n\frac{1}{x})^h\{\int d^2k_{\perp 1} V(k^2_\perp, k^2_{\perp 1}) \ldots \int d^2k_{\perp h} V(k^2_{\perp h-1}, k^2_{\perp h})\} \ . \tag{81}$$

Here $k^2_\perp$ is the qq transverse momentum in Fig. 23 and $k^2_\perp \simeq q^2$. The BFKL vertex

V above depends on the adjoining momenta in the ladder and is given by:

$$V(k^2_{\perp i-1}, k^2_{\perp i}) = \frac{c_A}{\pi}\alpha_s(k^2_{\perp i})\Big[\frac{k^2_{\perp i-1}}{k^2_{\perp i}|k^2_{\perp i-1} - k^2_{\perp i}|} - \gamma(k^2_{\perp i})\delta(k^2_{\perp i-1} - k^2_{\perp i})\Big] \quad , \tag{82}$$

where

$$\gamma(k^2_{\perp i}) = \int dk^2_\perp \frac{k^2_{\perp i}}{k^2_\perp}\Big\{\frac{1}{|k^2_\perp - k^2_{\perp i}|} - \frac{1}{[4k^4_\perp + k^4_{\perp i}]^{1/2}}\Big\} \quad . \tag{83}$$

Note that the above vertex reduces precisely to the three gluon vertex $V_{3g}(i)$ in the limit in which the transverse momenta are strongly ordered, so that $k^2_{\perp i-1} >> k_{\perp i}$:

$$V(k^2_{\perp i-1},\ k^2_{\perp i})\ \overrightarrow{k^2_{\perp i-1} >> k^2_{\perp i}}\ V_{3g}(i) = \frac{c_A}{\pi}\frac{\alpha_s(k^2_{\perp i})}{k^2_{\perp i}} \quad . \tag{84}$$

Because in Eq. (81) the transverse momenta $k^2_{\perp i}$ are **not** strongly ordered, the contribution in the curly bracket in this equation does not reduce simply to powers of the log-log of the virtual current momentum transfer q^2 [cf Eq. (76)]. One can, nevertheless, get some idea of what might be expected in the Regge region by considering a somewhat crude first approximation to $V(k^2_{\perp i-1}, k^2_{\perp i})$, in which one supposes that the dependence of $k^2_{\perp i-1}$ and $k^2_{\perp i}$ factorizes.[39] If the BFKL vertex were factorizable

$$V(k^2_{\perp i-1}, k^2_{\perp i}) = A(k^2_{\perp i-1})B(k^2_{\perp i}) \quad , \tag{85}$$

then the transverse momentum integrals in Eq. (81) are again trivial to do and the curly bracket in the equation reduced to

$$\{Eq.\ (81)\} = A(k^2_\perp)\lambda^h \quad , \tag{86}$$

where

$$\lambda = \int dk^2_{\perp i} A(k^2_{\perp i})B(k^2_{\perp i}) \quad . \tag{87}$$

In this approximation, the behaviour of $xg(x;q^2)$ in the Regge region is just

$$[xg(x;q^2)]^{\rm Regge} = A(q^2)\sum_h \frac{1}{h!}(\lambda\ \ell n\frac{1}{x})^h = \frac{A(q^2)}{x^\lambda} \quad . \tag{88}$$

If λ is positive, this is a singular behaviour as $x \to 0$, which again violates the Froissart bound of Eq. (80) since, for $q^2 = q_0^2$, $x \sim q_0^2/s$.

Although the actual BFKL vertex is not **factorable**, the result of the analysis of Balitsky Fadin Kuraev and Lipatov[44] shows that the gluon distribution function $xg(x;q^2)$ is given by a sum of terms of the above type, with various eigenvalues λ_i. The maximum eigenvalue in this sum then gives the most singular behaviour as $x \to 0$:

$$[xg(x;q^2)]^{\rm Regge} \underset{x\to 0}{\longrightarrow} \frac{A(q^2)}{x^{\lambda_{\rm max}}} \quad . \tag{89}$$

One can show, furthermore, that this maximum eigenvalue lies somewhere in the range

$$\frac{3.6}{\pi}\alpha_s(k_0^2) \geq \lambda_{\rm max} \geq \frac{12\ell n2}{\pi}\alpha_s(k_0^2) \tag{90}$$

where k_0^2 is some appropriate infrared cutoff, beyond which one cannot trust the calculation.[46]

The singular behaviour displayed at small x by the gluon distribution function of Eqs. (79) and (89) is an indication that the Altarelli Parisi equation (in the deep inelastic regime) and the BFKL equation (in the Regge regime) give an incomplete description of the physics at small x. Before trying to consider alternatives to these equations at small x, it is useful to try to understand physically what is the origin of the troubles one is encountering. A nice intuitive picture of what is happening has been put forth by Mueller.[47]

Consider for these purposes ep scattering in a frame where $xp >> \sqrt{q^2}$. Then a measurement of $g(x;q^2)$ probes gluons which have a transverse size $\Delta x_\perp \sim 1/\sqrt{q^2}$, but negligibile longitudinal size $\Delta x_{||} \sim 1/xp$. In this frame, one can ask how much of the area of the proton disk (πR^2) is occupied by gluons. If the gluons occupy an area much less than πR^2, as shown schematically in Fig. 24a, then the QCD parton model should be OK since - even at low x values - there is not much gluon overlap and one can sensible imagine that there are no additional contributions. If, on the other hand, the gluon density in the proton is very high, as shown schematically in Fig. 24b, then the parton picture idea that the external current probes just **one** constituent parton in the proton (and its descendants) ceases to be a sensible approximation and one must include further interactions.

The area occupied by the gluons is, approximately,

$$\begin{aligned} \text{Area glue} &\sim \text{transverse size.}\ \ \text{number gluons per}\ \frac{dx}{x} \\ &\sim \Delta x^2_\perp xg(x;q^2) \sim \frac{xg(x;q^2)}{q^2} \quad . \end{aligned} \tag{91}$$

So, as long as

$$\frac{xg(x;q^2)}{q^2} << \pi R^2 \quad , \tag{92}$$

one should be able to trust the results of the Altarelli Parisi or BFKL equations. However, when $xg(x;q^2) \simeq \pi R^2 q^2$, corresponding to the schematic picture of Fig. 24b, then the gluon density within the proton is so great that one must include more than the single ladders of Fig. 23 to account for the effects of the high gluon density.

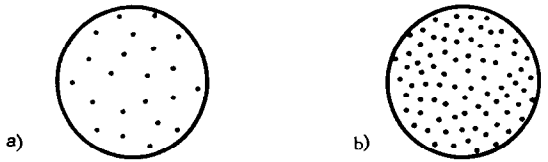

Figure 24: a) Sparse gluon distribution in the proton for which the Altarelli Parisi and BFKL equations hold; b) gluon distribution in proton which leads to important corrections to the simple ladder contributions.

When the inequality (92) is violated, it no longer makes sense to consider that under the probing of the virtual current a proton is "made up" of a linear chain of gluons, which are emitted independently but with well ordered momenta [c.f. Fig. 23]. At high gluon density effective gluon-gluon interactions are important which, in a Feynman graph language, correspond to having more than one gluonic chain participate when the virtual current V^* probes the proton.§ These effective gluon gluon interactions lead to modifications of the Altarelli Parisi and BFKL equations which serve to restore unitarity. The relevant equation which includes these important effects is known as the Gribov Levin Ryskin equation (GLR equation) and was derived in the early 1980's by these authors.[39]

Before discussing the GLR equation, it is interesting to see for what values of x and q^2 one gets into trouble, as a result of Eq. (92) not being satisfied. For definitiveness, let us consider the deep inelastic low x region where the gluon distribution is given by Eq. (79). Setting $xg(x;q^2)$ in Eq. (79) equal to $\pi R^2 q^2$ determines the region in $x - q^2$ space where effective gluon-gluon interactions become important. As is easily seen, this region is essentially a parabola in the $\ell n\ 1/x - \ell n\ q^2$ plane given by the equation

$$\ell n\ 1/x = \left[\frac{\pi b}{4c_A}\frac{1}{\ell n\ \ell n q^2/\Lambda^2}\right]\ell n^2(\pi R^2 q^2)\,. \qquad (93)$$

The quantity in the square brackets above in the HERA energy range is of the order of 0.2. Fig 25 shows the intersection of the line given by Eq. (93) for two values of R [$R = 5\ GeV^{-1}$ and $R = 2\ GeV^{-1}$] which as we shall see below are sensible, along with the kinematical region accessible at HERA. For regions to

§That is, the current V^* resolves more than one gluon (and its descendants) in the proton.

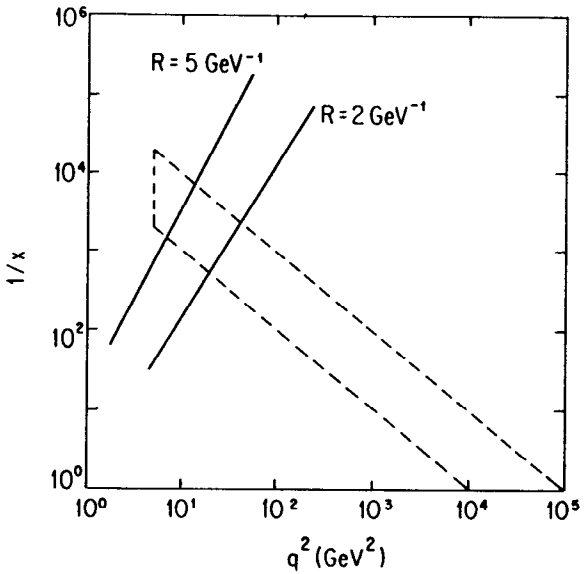

Figure 25: Kinematical region accessible to HERA. The diagonal lines correspond to a solution of Eq. (93), so that to the left of these lines multiparton interactions should begin to become important.

the left of the diagonal lines the multi parton interactions should begin to be important. Obviously, in this respect HERA is a very interesting machine, for it will begin to probe this new kinematical regime.

After this qualitative discussion, let us begin to consider more seriously how the very singular behaviour as $x \to 0$ in the Altarelli Parisi and BFKL equations [c.f. Eqs. (79) and (89)] gets fixed. What cures the very singular $x \to 0$ behaviour in these equations is the incorporation of more than one gluon ladder (and the interaction of the gluons in these ladders) to describe the partonic content of the proton. These further contributions give a shadowing correction to the original very singular behaviour of $xg(x;q^2)$ as $x \to 0$, yielding finally a function which is better controlled in this region.

In diagrammatic language, the shadowing corrections arise from the Feynman graphs shown in Fig. 26, in which one is instructed to take the discontinuity coming from all the possible cuts. These graphs lead to a decrease in the growth of $xg(x;q^2)$ as $x \to 0$, with this function eventually reaching some limiting distribution for extremely low x values. The precise value of this limiting distribution is, however, not a matter that is totally resolved, because as $x \to 0$ further corrections beyond those shown in Fig. 26 can intervene. ¶ Mueller,[47] for instance,

¶These corrections correspond to probing multigluon states ($N_g > 2$) and their associated ladders in the proton.

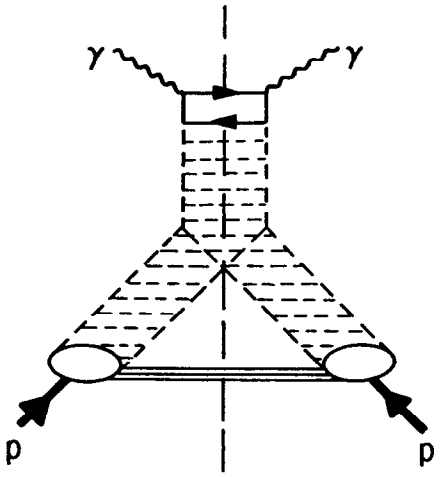

Figure 26: Ladder interactions whose effect is to shadow the singular contribution as $x \to 0$ coming from the contributions of a single ladder.

argues on the basis of the Froissart bound[42] that as $x \to 0$ the gluon distribution should approach

$$xg(x;q^2) \;\; \overrightarrow{x \to 0} \;\; q^2R^2 \;\; h(x;q^2) \qquad (94)$$

with $h(x;q^2)$ being weakly dependent on x and q^2, with perhaps $h(x;q^2) \sim \ell n^2 1/x$.

The ladder diagrams of Fig. 23 lead to either the BFKL or the Altarelli Parisi equations, depending on what the assumed vertices and transverse momentum orderings are. Including the diagrams of Fig. 26 leads to a **nonlinear** modification of these equations, whose principal characteristic is to damp away the unphysical behaviour at low x. The inclusion of the diagrams of Fig. 26 is what gives rise to the Gribov Levin Ryskin equation. In this equation,[39] at small x a new fundamental object becomes important for the description of the relevant physical phenomena: the triple ladder vertex shown in Fig. 26.

To understand the role of the triple ladder vertex, it is useful to give a pictorial description of the Altarelli Parisi equation for the gluon distribution function. The differential form of the equation, given in Eq. (69), is easily seen to be equivalent to the following integral equation

$$xg(x;q^2) = xg(x;q_0^2) \; + \; \int^{q^2} \frac{dk_\perp^2}{k_\perp^2} \int_x^1 \frac{d\xi}{\xi} \frac{c_A}{\pi} \alpha_s(k_\perp^2) \xi g(\xi;k_\perp^2) \;\; , \qquad (95)$$

where $xg(x;q_0^2)$ is some input gluon distribution. This integral equation associates diagramatically $xg(x;q^2)$ to the graph of Fig. 27a, while the second term of Eq. (95) corresponds to the graph of Fig. 27b, in which there is an extra gluon rung.

The diagram of Fig. 26 - which because of its shape has become known as a fan diagram - corresponds to the (first) non linear modification to Eq. (95). To the right hand side of Eq. (95) one must add the contribution of the fan diagram, shown more schematically in Fig. 28. Note that, as I already mentioned earlier on, since in the fan diagram there is more than one way to take the discontinuity, the resulting contribution to $xg(x;q^2)$ is the sum of all these discontinuities. A rather involved computation[39 48] secures the following contribution to $xg(x;q^2)$ coming from the fan diagram:

$$[xg(x;q^2)]_{\rm Fan} \; = \; - \int^{q^2} \frac{dk_\perp^2}{k_\perp^2} \int_x^1 \frac{d\xi}{\xi} \frac{c_A}{\pi} \alpha_s(k_\perp^2) V_{TL}(k_\perp^2) [\xi g(\xi;k_\perp^2)]^2 \;\; , \qquad (96)$$

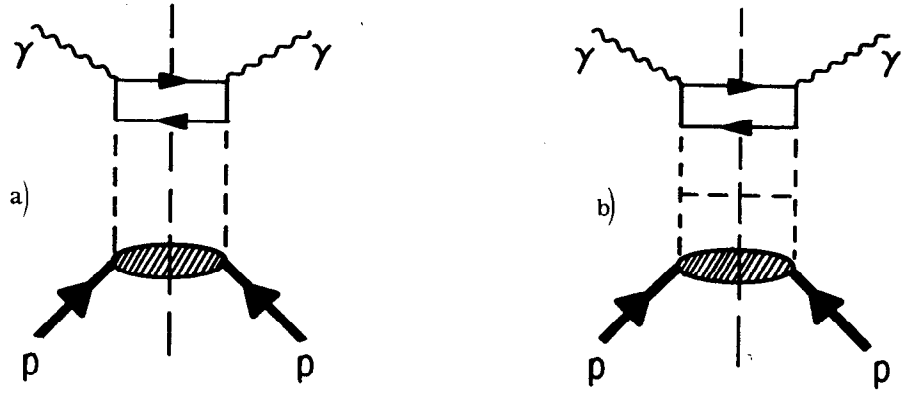

Figure 27: a) Pictorial representation of $xg(x;q^2)$ and of b) its one gluon interaction.

where the triple ladder vertex $V_{TL}(k_\perp^2)$ above is given by

$$V_{TL}(k_\perp^2) \; = \; \frac{9\pi}{16} c_A \alpha_s(k_\perp^2) \Big(\frac{1}{R^2 k_\perp^2} \Big) \;\; . \qquad (97)$$

Various remarks are in order:

i) The contribution of the fan diagram depends - rather naturally not on $xg(x;q^2)$ but its **square**. So this contribution is negligible in physical circumstances (and kinematical regions) where the gluon density in the proton is low, like in Fig. 24a. However, this becomes important when this density starts to grow and one arrives at the situation schematically depicted in Fig. 24b.

ii) Because of the **minus** sign in Eq. (96), the non linearities associated with the fan diagram indeed serve to damp the unphysical behaviour of $xg(x;q^2)$ at low x. The presence of this sign is the result of the shadowing of one ladder by another and is characteristic of absorptive phenomena where unitarity comes into play.‖

iii) The triple ladder vertex $V_{TL}(k_\perp^2)$ contains an **incalculable** radius parameter R. This parameter is associated with the momentum flow along the gluon ladders in Fig. 28, which gives rise to an infrared sensitive integral which must be cut off at some scale. One can proffer arguments for R lying somewhere in the range[47]

$$2\ GeV^{-1} < R < 5\ GeV^{-1}\ , \tag{98}$$

with the lower limit above being associated with the size of a valence quark and the upper limit being given by the size of a nucleon.

iv) The fan diagram contribution is a higher twist effect, since the triple ladder vertex gives an extra contribution of $\frac{1}{k_\perp^2}$. This is most easily seen by considering the ℓnq^2 derivative of the fan diagram contributions

$$\frac{d}{d\ \ell n\ q^2}[xg(x;q^2)]_{\rm Fan} = -\frac{9c_A^2\alpha_s^2(q^2)}{16q^2R^2}\int_x^1 \frac{d\xi}{\xi}[\xi;g(\xi,q^2)]^2\ . \tag{99}$$

If one includes the contribution of the fan diagrams, the gluon distribution function no longer satisfies the Altarelli Parisi equation (or the BFKL equation in the Regge region) but a non linear integro differential equation - the Gribov Levin Ryskin (GLR) equation. For the gluon distribution in the deep inelastic, low x region, this equation takes the form:

$$\begin{aligned}\frac{d}{d\ \ell n\ q^2}[xg(x;q^2)] &= \frac{c_A\alpha_s(q^2)}{\pi}\int_x^1 \frac{d\xi}{\xi}[\xi g(\xi;q^2] \\ &- \frac{9c_A^2\alpha_s^2(q^2)}{16R^2q^2}\int_x^1 \frac{d\xi}{\xi}[\xi g(\xi;q^2)]^2\ .\end{aligned} \tag{100}$$

‖For further discussion of this point, see[48] and, particularly,[39]

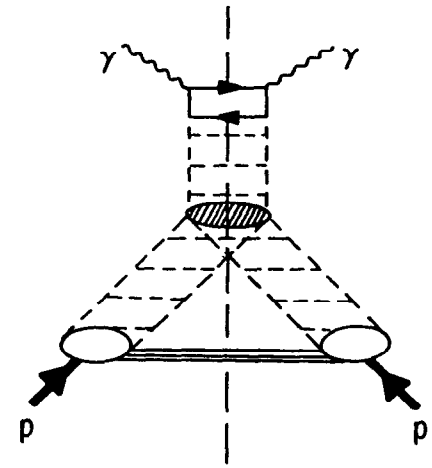

Figure 28: Schematic representation of the fan diagram which include the triple ladder vertex V_{TL}. Note that all cuts through the ladders must be taken to obtain Eq. (96).

The second contribution on the RHS above comes precisely from the fan diagrams [c.f. Eq. (99)]. This equation has been analyzed recently numerically by Collins and Kwiecinski[49] and by Bartels Blümlein and Schuler[50] and I will discuss here some of their results. Fig. 29, taken from,[49] shows how the inclusion of the fan diagram contribution modifies the small x behaviour of the gluon distribution function considerably. Furthermore the amount of shadowing clearly depends on the scale one assumes for the radius parameter R.

Similar results to those discussed by Collins and Kwiecinski[49] have been obtained by Bartels et al who also included shadowing corrections via the GLR equation. Fig. 30 shows their results for the gluon distribution function in two q^2 regions and for two rather distinct x regions. For $x \sim 10^{-3} - 10^{-5}$ the shadowing effect computed by Bartels et al is qualitatively similar to that shown in Fig. 29. However, for extremely low values of x ($x \leq 10^{-15}$) the gluon distribution actually appears to **saturate** to some nearly x independent, but q^2 dependent value. The saturation of the gluon distribution function at the very small x values shown in Fig. 30 should be taken with a grain of salt. Saturation, roughly speaking, means that the quadratic term in g in Eq. (100) are of the order of the linear terms. But when this happens one cannot neglect higher nonlinearities, i.e., fan diagrams with multiladders proportional to $[\xi g(\xi;q^2)]^{N_g}$. For small, but not extremely small x, the ratio of the quadratic to the linear term in the GLR equation is still sensible,

as Fig. 31 shows. However, this same ratio would begin to go out of control as x becomes very small.

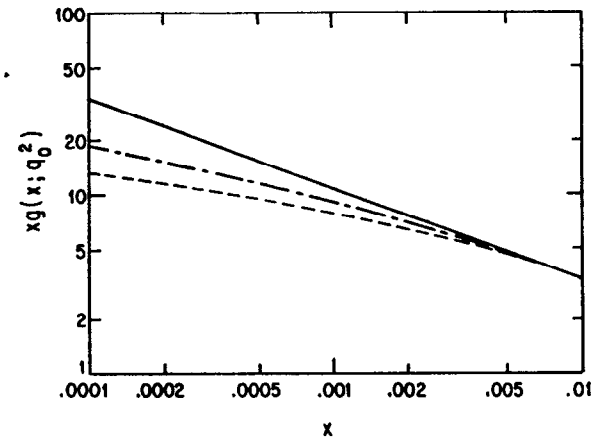

Figure 29: Plot of $xg(x;q^2)$ versus x for three differrent assumptions. The solid line is the result of the Altarelli Parisi equation, while the dash-dotted and dashed lines incorporate shadowing with $R = 5\ GeV^{-1}$ and $R = \frac{5}{\sqrt{2}}\ GeV^{-1}$ in the GLR equation. [49]

Although the results shown in Fig. 29 and 30 are quite interesting, it is important to note that the actual results one obtains are rather sensitive to what equation and what input distributions one uses, as well as the strength one assumes for the nonlinearities in Eq. (100). This salutory lesson emerges clearly from the study of Bartels et al. For instance, Fig. 32 shows that the differences between the Altarelli Parisi equation with the simplified low x structure for the gluon-gluon splitting function and the full Altarelli Parisi equation is comparable to the effect of including the first nonlinearities in the simplified equation through Eq. (100)! Similarly, by taking different input distribution functions at some low q^2 value (normally $q_0^2 = 4\ GeV^2$), one obtains quite different amount of shadowing. As it is physically clear, the more singular the input function is, the more shadowing one is to expect. This is illustrated in Fig. 33 for two radically different input distributions. The Morfin-Tung[51] distribution function is singular as $x \to 0$

$$[xg(x;q_0^2)]_{MT} \sim \frac{1}{x^{0.33}} \tag{101}$$

while the input distribution of Eichten et al.[52] is x independent:

$$[xg(x;q_0^2)]_{EHLQ} \sim \text{const}\ . \tag{102}$$

As a result, as is demonstrated in Fig. 33, the former distribution function has considerably stronger modifications at small x, as a result of shadowing.

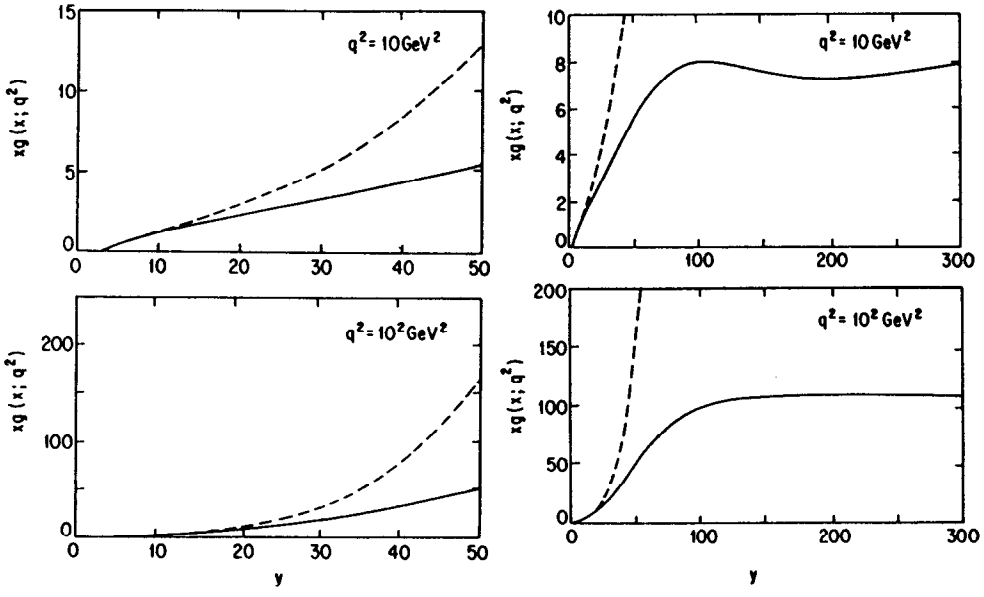

Figure 30: Plots of $xg(x;q^2)$ for two different values of q^2, as a function of $y \simeq 6.6\ \log_{10}(\frac{1}{x})$. The dashed line is the result of the Altarelli Parisi equation while the solid line gives the result of the GLR equation. Note how, for extremely low values of x, the gluon distribution function saturates.[50]

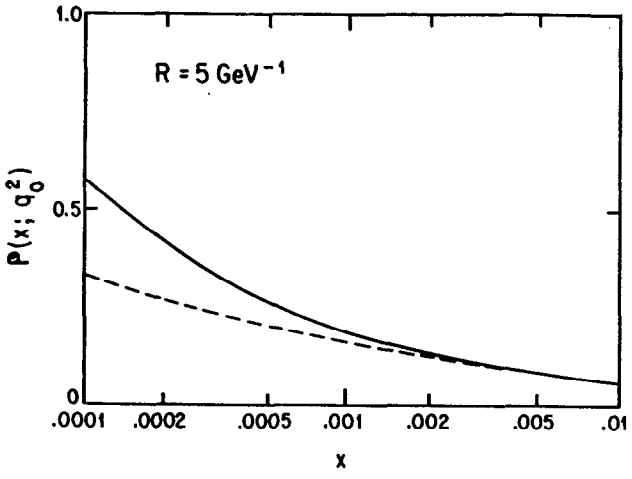

Figure 31: Plot of the ratio $P(x;q_0^2)$ which measures the size of the quadratic gluon contribution compared to the gluon contribution itself in Eq. (100), for the case when no shadowing is taken into account (solid line) and when shadowing is included (dashed line). Here $q_0^2 = 4\ GeV^2$ and $R = 5\ GeV^{-1}$. [49]

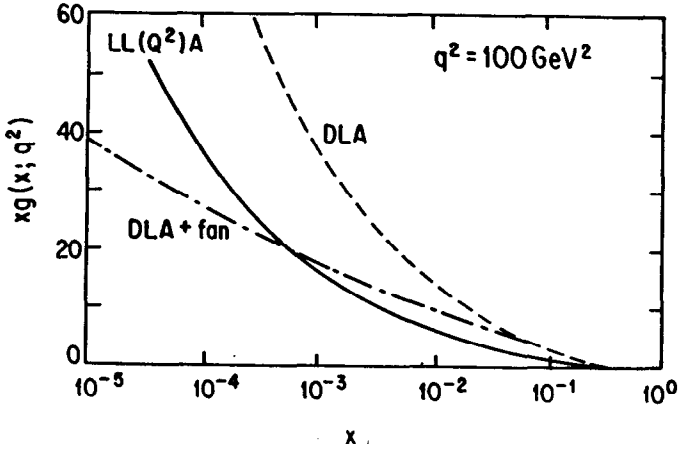

Figure 32: Comparison between the gluon distribution functions obtained by using the simplified Altarelli Parisi equation Eq. (69) [DLA], the full Altarelli Parisi equation $[LL(Q^2)A]$ and the GLR equation, Eq. (100) [DLA + fan]. [50]

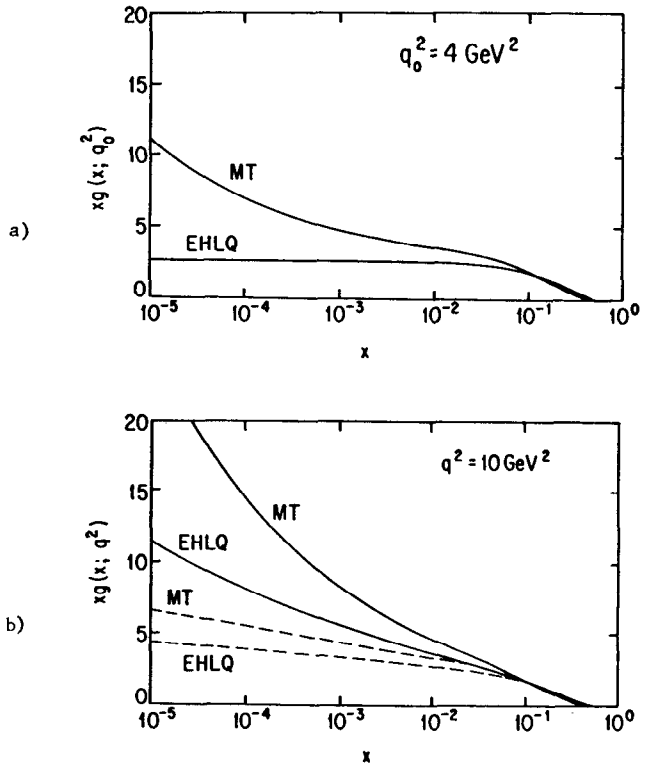

Figure 33: Comparison of shadowing for different input distribution functions: a) The input distributions of Morfin and Tung[51] and Eichtein et al.[52] at $q_0^2 = 4\ GeV^2$; b) The evolved distributions including (dashed lines) and excluding (solid lines) shadowing.[50]

The above discussion points to the need of further experimental and theoretical input before one can hope to really understand the low x behaviour of the gluon (and quark) distribution functions. This point emerges very clearly from a recent paper of Kwiecinski, Martin, Stirling and Roberts.[53] These authors have done a careful reanalysis of the structure functions at low x and have considered their evolution to larger q^2. The study of Kwiecinski et al.[53] was based on the GLR equation in which the full splitting functions - including corrections of $0(\alpha_s)$ - are used. Furthermore, for low q^2 and small x the linear term in the GLR equation used is precisely that of the BFKL equation. The result of their analysis is that present day data is incapable of distinguishing between input gluon distribution functions which are singular and those which are not. This is illustrated clearly in Fig. 34 where the BCDMS data for F_2 is obviously fit equally well by either the B_- or B_0 curve. These curves are generated by evolving $xg(x;q_0^2)$ from two rather different input gluon distributions. In the case of the B_0 curve, the input gluon distribution at $q_0^2 = 4\ GeV^2$ has a non singular behaviour as $x \to 0$[53]:

$$xg(x;q_0^2) \;=\; 2.87\ (1-x)^{5.1} \quad (\text{set } B_0)\ . \tag{103}$$

The B_- set on the other hand, at $q_0^2 = 4\ GeV^2$ behaves as $x^{-1/2}$ as $x \to 0$:

$$xg(x;q_0^2) \;=\; \frac{0.265[1+20x](1-x)^{5.5}}{x^{1/2}} \quad (\text{set B}_-)\ . \tag{104}$$

Although both the B_- and B_0 sets fit the existing data equally well, they begin to depart from each other at values of $x \leq (2-5)\times 10^{-3}$. In both sets the effects of shadowing are beginning to be felt in the HERA range, although numerically the singular set with shadowing, using $R = 2\ GeV^{-1}$, gives roughly the same contribution as that of the unshadowed non singular set!** This is shown in Fig. 35, both for $F_2(x;q^2)$ and for the longitudinal structure function $F_L(x;q^2)$. Because HERA will be able to measure $xg(x;q^2)$ at small x, it is clear that it will give important new input information for extrapolating these structure functions to the even smaller x's of interest for the LHC and the SSC. Furthermore, if at HERA one could also measure $xg(x;q^2)$, for different values of q^2 one could already get some information on how important the shadowing is in the q^2 evolution.

In Section 2 we already discussed various ideas of how to extract $xg(x;q^2)$ at HERA from measurements of $F_L(x;q^2)$ and by studying heavy quark production, both at the ψ and in the continium. As a last topic in these lectures I want to briefly return to this issue - particularly as it concerns the measurement of $xg(x;q^2)$ from heavy quark production. The main formula for $Q\bar{Q}$ production which we used in our earlier discussion was based on the lowest order graph for photon gluon fusion, shown in Fig. 36a, which yields

$$\sigma_{\gamma p} = \frac{7}{9}\pi\alpha_s\alpha\frac{e_Q^2}{M_Q^2}[x_g g(x_g;Q^2)]\Big|_{\substack{Q^2 \simeq M_Q^2 \\ x_g \simeq \frac{4M_Q^2}{s_{\gamma p}}}}\ . \tag{105}$$

**This kind of ambiguity is similar to the one found earlier by.[50]

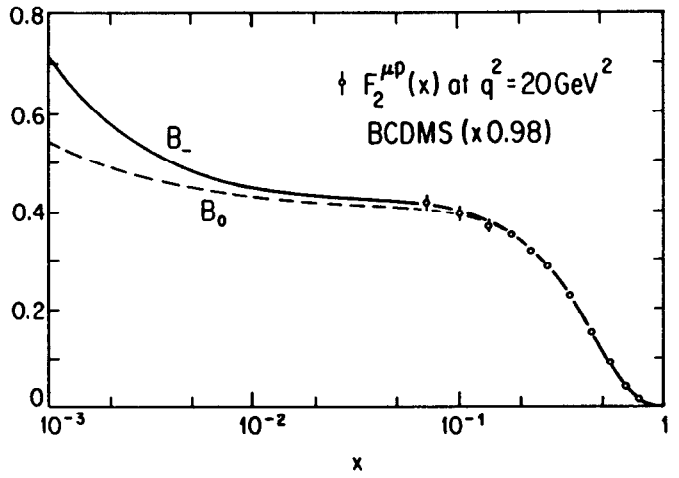

Figure 34: Fit to to $F_2(x)$ at $q^2 = 20\ GeV^2$ using as inputs the gluon distributions of either the B_- set or B_0 set. [53]

This formula can be perturbatively improved by calculating the $0(\alpha_s)$ corrections, and this was done by Ellis and collaborators[32,34] However, as we discussed in this Section, since one is interested really in the low x behaviour, one should really sum the whole set of gluon ladders, shown in Fig. 36b, which build up the small x behaviour of the gluon distribution function.

Catani, Ciafaloni and Hautmannn[35] have pointed out, however, that the inclusion of the gluon ladders does not simply replace $x_g g(x_g;Q^2)$ in the naive formula (105) by an "improved" gluon distribution, such as would emerge from solving the Altarelli Parisi equation (95) or its improvement, the GLR equation, Eq. (100). Rather, the inclusion of the ladders of fig. 36b results in a formula for $\sigma_{\gamma p}$ which, more correctly, involves a $k_\perp$-space convolution:

$$\sigma_{\gamma p} = \frac{1}{4M_Q^2}\int dk_\perp^2 \int_0^1 \frac{d\xi}{\xi}\hat{\sigma}(\frac{x_g}{\xi};k_\perp)F(\xi;k_\perp)\ . \tag{106}$$

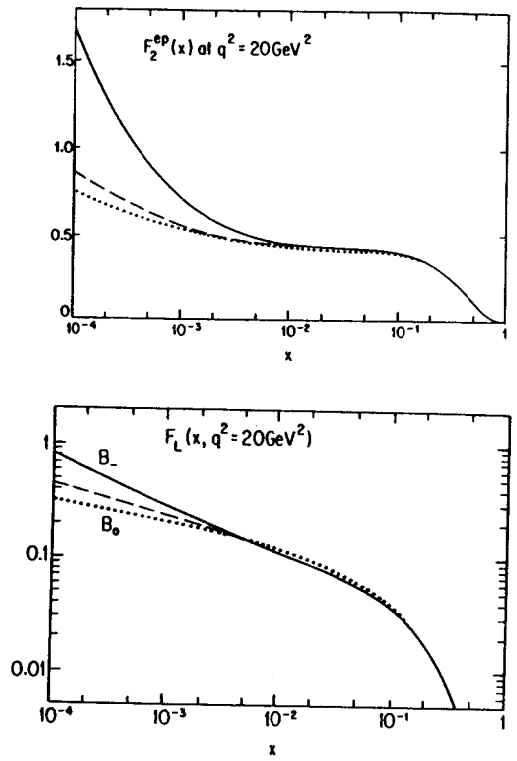

Figure 35: Expectation for the structure functions $F_2(x;q^2)$ and $F_L(x;q^2)$ in the HERA energy range using the B_- set (unshadowed-solid line; with shadowing $[R = 2\ GeV^{-1}]$-dashed line) and the B_0 set (unshadowed-dotted line). [53]

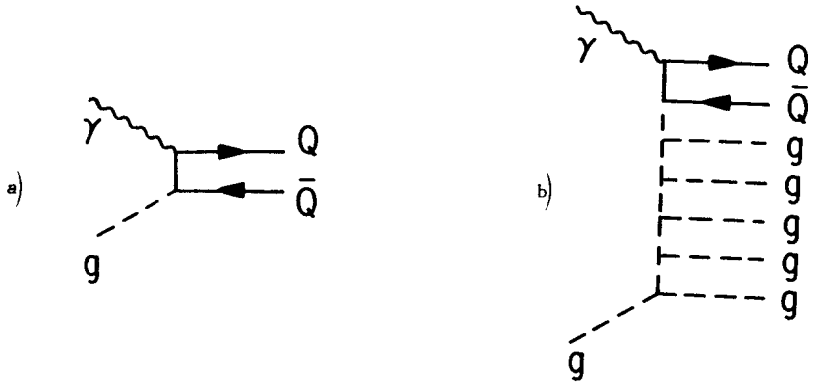

Figure 36: a)Lowest order photon gluon fusion graph for $Q\bar{Q}$ production; b) gluon chain entering in photon gluon fusion which builds up the small x behaviour of $xg(x;Q^2)$.

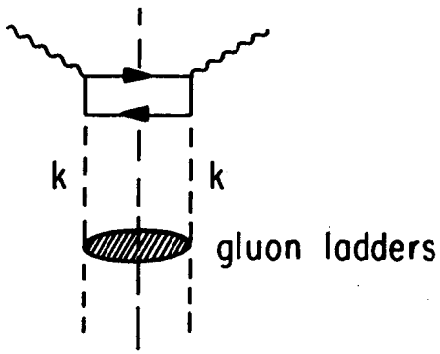

Figure 37: Diagramatic representation of Eq. (106).

Here $\hat{\sigma}$ is the cross section for $\gamma g(k) \to Q\bar{Q}$ in which the gluons have a transverse momentum $k_\perp$ and F is related to the gluon structure function, when one integrates it over $k_\perp^2$:

$$xg(x;Q^2) = \int^{Q^2} dk_\perp^2 F(x;k_\perp) \; . \tag{107}$$

Figure 37 shows a pictorial representation of Eq. 106.

Because of the $k_\perp$ convolution of Eq. (106), the final result for $\sigma_{\gamma p}$ is not simply given by replacing the gluon distribution function in Eq. (105) by its "improved" version at small x. Rather the $k_\perp$ convolution produces an effective K-factor, whose magnitude can in fact be very large. For example, if one uses a gluon distribution corresponding to the solution of the BFKL equation

$$x_g g(x_g;q_0^2)\Big|_{BFKL} \sim \frac{A(q_0^2)}{x_g^{\lambda_{\max}}} \tag{108}$$

the K-factor calculated by Catani, Ciafaloni and Hautmann[35] is $K_{BFKL} = \frac{27}{56}\pi^2$, which is indeed large. Of course, with enough data it may be possible to undo the convolution in Eq. (106) by studying the transverse momentum distribution of the produced heavy quarks. Nevertheless, this discussion makes it clear that, although HERA will provide invaluable information on the gluon distribution function at small x, considerable further theoretical analysis will be necessary before this function can be unambiguously extracted from the data.

Acknowledgement:

I am grateful for the hospitality of the Aspen Center for Physics, where these lectures were prepared. Discussions with Reinhold Rückl there on HERA physics were extremely helpful and are happily acknowledged. This work was supported in part by the Department of Energy under contract No. DE-AT03-88ER 40383 Mod A006- Task C.

References

1. S. Drell, these proceedings
2. For a general discussion of QCD, see, for example, the following monographs: T. Muta **Foundations of Quantum Chromodynamics** (World Scientific, Singapore 1987); R. Field **Applications of Perturbative QCD** (Addison Wesley, Redwood City, California, 1989). Useful reviews of QCD include, G. Altarelli, Phys. Rept. 81 (1982) 1; R. K. Ellis, Proceedings of the Santa Fe TASI, ed. R. Slansky and G. West (World Scientific, Singapore 1987)
3. J. D. Bjorken and E. A. Paschos, Phys. Rev. 185 (1969) 1975; R. P. Feynmann **Photon Hadron Interactions** (Benjamin, Reading, Mass 1972)
4. J. D. Bjorken, Phys. Rev. 179 (1969) 1547
5. D. Amati and G. Veneziano, Nucl. Phys. B140 (1978) 54; R. K. Ellis, H. Georgi, M. Machacek, H. D. Politzer and G. G. Ross Nucl. Phys. B152 (1979) 285; A. V. Efremov and A. V. Radyushkin, Sov. Theor. Math. Phys. 44 (1980) 17; S. Libby and G. Sterman, Phys. Rev. D18 (1978) 3252; A. Mueller, Phys. Rev. D18 (1978) 3705.
6. For recent reviews, see for example J. C. Collins and D. Soper, Ann. Rev. Nucl. Part. Sci. 37 (1987) 383; J. C. Collins, D. E. Soper and G. Sterman, in **Perturbative QCD** ed. A. H. Mueller (World Scientific, Singapore 1990)
7. G. Altarelli and G. Parisi, Nucl. Phys. B126 (1977) 298; for earlier work in the same direction, see also Yu. L. Dokshitzer, JETP 73 (1971) 1216; V. N. Gribov and L. N. Lipatov, Sov. J. Nucl. Phys. 15 (1972) 78
8. For a discussion, see for example, A. J. Buras, Rev. Mod. Phy. 52 (1980) 199
9. P. Berge et al, Zeit. Phys. C49 (1991) 187
10. T. Hansl Kozanecka, these proceedings
11. S. Mishra, these proceedings
12. W. A. Bardeen, A. J. Buras, D. W. Duke and T. Muta, Phys. Rev. D18 (1978) 3998
13. G 't Hooft, Nucl. Phys. B61 (1973) 455
14. M. Diemoz, F. Ferroni, E. Longo and G. Martinelli, Zeit. Phys. C39 (1988) 21
15. BCDMS Collaboration, A. C. Benvenuti et al, Phys. Lett. B195 (1987) 91, 97; B223 (1989) 485, 490
16. G. Altarelli, Ann. Rev. Nucl. Part. Sci. 39 (1989) 357
17. P. N. Harriman, A. D. Martin, W. J. Stirling and R. G. Roberts, Phys. Rev. D42 (1990) 798
18. EMC Collaboration, J. J. Aubert et al, Nucl. Phys. B259 (1985) 189; M. Arneodo et al, Nucl. Phys. B333 (1990) 1

19. M. Bonesini et al, Zeit. Phys. C 38 (1988) 371
20. NMC Collaboration, D. Allasia et al, Phys. Lett. B294 (1990) 366
21. J. Blümlein, M. Klein, G. Ingelman and R. Rückl, Zeit Phys. C45 (1990) 501
22. C. Callan and D. Gross, Phys. Rev. Lett. 22 (1969) 156
23. A. Zee, F. Wilczek and S. B. Treiman, Phys. Rev. D10 (1974) 2881; D. V. Nanopolous and G. G. Ross, Phys. Lett. 588 (1975) 105; E. Witten, Nucl. Phys. B 120 (1977) 189. For a derivation starting from the Altarelli Parisi equations, see G. Altarelli and G. Martinelli, Phys. Lett. 76 B (1978) 89
24. A. D. Martin, R. G. Roberts and W. J. Stirling, Phys. Rev. D37 (1988) 1161
25. J. L. Miramontes, M. A. Miramontes and J. Sanchez Guillen, Phys. Rev. D40 (1989) 2185
26. A. M. Cooper Sarkar et al., Zeit. Phys. C39 (1988) 281
27. A. D. Martin, C. K. Ng and W. J. Stirling, Phys. Lett. B191 (1987) 200
28. M. Tkaczyk, W. J. Stirling and D. H. Saxon, Proceedings of the HERA Workshop, Hamburg 1987, ed. R. D. Peccei (DESY, Hamburg 1987)
29. Z. Kunszt and W. J. Sterling, Phys. Lett. B217 (1989) 563
30. R. S. Fletcher, F. Halzen and R. W. Robinett, Phys. Lett. B225 (1989) 1
31. W. Kwong, P. MacKenzie, R. Rosenfeld and J. Rosner, Phys. Rev. D37 (1988) 3210
32. R. K. Ellis and Z. Kunzst, Nucl. Phys. B303 (1988) 653
33. G. Ingelman and G. A. Schuler, Zeit. Phys. 640 (1988) 299
34. R. K. Ellis and P. Nason, Nucl. Phys. B 312 (1989) 551
35. S. Catani, M. Ciafaloni and F. Hautmann, Phys. Lett. B242 (1990) 97
36. G. Schuler, Proceedings of the 5th Workshop of the INFN Eloisatron Project, Erice, Italy 1988, ed. A. Ali. See also K. J. Abrahams, H. Jung, G. A. Schuler and J. F. de Troconiz, Proceedings of the ECFA Workshop on the LHC, Aachen, Germany 1990.
37. K. J. Abrahams, H. Jung, G. A. Schuler and J. F. de Troconz, Proceedings of the ECFA Workshop on the LHC, Aachen, Germany 1990.
38. E. M. Levin and M. G. Ryskin, Nucl. Phys. B. (Proc. Suppl) 18C (1990) 92
39. L. V. Gribov, E. M. Levin and M. G. Ryskin, Phys. Rept. 100 (1983) 1
40. For a discussion, see for example, G. Altarelli, Phys. Rept. 81 (1982) 1
41. For a more thorough treatment, see R. Field **Application of Perturbative QCD** (Addison Wesley, Redwood City, California, 1989)
42. M. Froissart, Phys. Rev. 123 (1961) 1053
43. L. N. Lipatov, Yad. Fiz 23 (1976) 642 [Sov. J. Phys. 23 (1976) 338]
44. E. A. Kuraev, L. N. Lipatov and V. S. Fadin Zh. Eksp. Teor. Fiz 72 (1977) 373 [Sov. Phys. JETP 45 (1977) 199]; Phys. Lett. 60B (1975) 50; Ya. Balitsky and L. N. Lipatov, Yad. Fiz 28 (1978) 1597 [Sov. J. Nucl. Phys. 28 (1978) 822]
45. F. E. Low, Phys. Rev. D12 (1975) 163; S. Nussinov, Phys. Rev. Lett. 34 (1975) 1286, Phys. Rev. D14 (1976) 246
46. J. C. Collins and J. Kwiecinski, Nucl. Phys. B316 (1989) 307
47. A. H. Mueller, Nucl. Phys. B (Proc. Suppl.) 18C (1990) 125; Nucl. Phys. B 307 (1988) 34; B317 (1989) 573; B 335 (1990) 115
48. A. H. Mueller and J. Qiu, Nucl. Phys. B 268 (1986) 427
49. J. C. Collins and J. Kwiecinski, Nucl. Phys. B 35 (1990) 89
50. J. Bartels, J. Blümlein and G. A. Schuler, Nucl. Phys. B (Proc. Suppl.) 18C (1990) 147
51. J. G. Morfin and W. K. Tung, Z. Phys. 52(1991) 13
52. E. Eichten et al, Rev. Mod. Phys. 56 (1984) 579; E 58 (1986) 1065
53. J. Kwiecinski, A. D. Martin, R. G. Roberts and W. J. Stirling, Phys. Rev. D 42 (1990) 3645